

November 19, 2024

# Data-driven results for light-quark connected and strange-plus-disconnected hadronic $g - 2$ short- and long-distance windows

Genessa Benton<sup>a</sup>, Diogo Boito<sup>b</sup>, Maarten Golterman<sup>c</sup>, Alexander Keshavarzi<sup>d</sup>,  
Kim Maltman<sup>e,f</sup>, and Santiago Peris<sup>g</sup>

<sup>a</sup>*Department of Physics, University of Illinois, Urbana, IL 61801, USA*

<sup>b</sup>*Instituto de Física de São Carlos, Universidade de São Paulo, CP 369,  
13560-970, São Carlos, SP, Brazil*

<sup>c</sup>*Department of Physics and Astronomy, San Francisco State University, San  
Francisco, CA 94132, USA*

<sup>d</sup>*Department of Physics and Astronomy, The University of Manchester,  
Manchester M13 9PL, United Kingdom*

<sup>e</sup>*Department of Mathematics and Statistics, York University, Toronto, ON  
Canada M3J 1P3*

<sup>f</sup>*CSSM, University of Adelaide, Adelaide, SA 5005 Australia*

<sup>g</sup>*Department of Physics and IFAE-BIST, Universitat Autònoma de Barcelona,  
E-08193 Bellaterra, Barcelona, Spain*

## Abstract

A key issue affecting the attempt to reduce the uncertainty on the Standard Model prediction for the muon anomalous magnetic moment is the current discrepancy between lattice-QCD and data-driven results for the hadronic vacuum polarization. Progress on this issue benefits from precise data-driven determinations of the isospin-limit light-quark-connected (lqc) and strange-plus-light-quark-disconnected (s+lqd) components of the related RBC/UKQCD windows. In this paper, using a strategy employed previously for the intermediate window, we provide data-driven results for the lqc and s+lqd components of the short- and long-distance RBC/UKQCD windows. Comparing these results with those from the lattice, we find significant discrepancies in the lqc parts but good agreement for the s+lqd components. We also explore the impact of recent CMD-3  $e^+e^- \rightarrow \pi^+\pi^-$  cross-section results, demonstrating that an upward shift in the  $\rho$ -peak region of the type seen in the CMD-3 data serves to eliminate the discrepancies for the lqc components without compromising the good agreement between lattice and data-driven s+lqd results.

# 1 Introduction

In 2021 and 2023, the Fermilab E989 experiment published new measurements [1–3] of the anomalous magnetic moment of the muon,  $a_\mu$ . The new results are compatible with the older, less precise, BNL E821 determination [4] and produce a new experimental  $a_\mu$  world average with an impressive precision of 0.19 ppm. Prior to the release of the E989 results, in 2020, the Muon  $g - 2$  Theory Initiative published a White Paper [5] giving the then-best Standard Model (SM) prediction for  $a_\mu$ , based on the results of Refs. [6–29]. This prediction, which employed the then-current data-driven result for the hadronic vacuum polarization (HVP) contribution, was in disagreement with the new experimental result.

Since the 2020 White Paper, three important developments have taken place. First, in 2021, the BMW collaboration published a complete and competitive lattice-QCD determination of the HVP contribution,  $a_\mu^{\text{HVP}}$ , to  $a_\mu$  [30]. The modified SM prediction produced by this result is in agreement with experiment within less than  $2\sigma$ .<sup>1</sup> Second, new experimental results for the cross section of  $e^+e^- \rightarrow \pi^+\pi^-$  obtained by the CMD-3 experiment [32] were found to produce a  $2\pi$  contribution to  $a_\mu^{\text{HVP}}$  significantly larger than that implied by previous experiments [5], raising further questions about the data-driven evaluation. Finally, very recently, in Ref. [33], a more precise determination of  $a_\mu^{\text{HVP}}$  was obtained using new BMW lattice-QCD results combined with a data-driven evaluation, based on Ref. [12], of the long-distance contribution from a region in Euclidean time where the lattice-QCD determination is significantly less precise. This leads to a result for  $a_\mu$  that agrees with experiment to within less than  $1\sigma$ .

Given this situation, it has become critical to understand the present discrepancy between the data-driven and lattice-QCD results for  $a_\mu^{\text{HVP}}$  in more detail. An important tool for the comparison between lattice-QCD and data-driven results is the method of “windows,” introduced by RBC/UKQCD [34]. The method involves splitting the  $a_\mu^{\text{HVP}}$  integral in three parts with a short-, an intermediate-, and a long-distance contribution. For the intermediate window, which significantly suppresses lattice uncertainties associated with the continuum limit and finite volume effects, and which can be computed with very good statistical precision, it has been shown that the data-driven approach and the lattice-QCD results display a significant tension, of about  $4\sigma$  [35, 36].<sup>2,3</sup> Since the lattice intermediate window result is the sum of a number of different components, it is of interest to further refine this comparison in order to clarify the origin of the observed discrepancy.

The ingredients that go into the lattice determination are as follows. The main contribution arises from the isospin-symmetric light-quark connected diagrams, followed in size by the strange-quark connected and three-flavor disconnected contributions.

---

<sup>1</sup>An early sign of discrepancy between lattice QCD and the data-driven approach was the light-quark connected RBC/UKQCD intermediate-window lattice result of Ref. [31], which was significantly larger than a data-driven estimate.

<sup>2</sup>This result predates the publication of the new CMD-3 measurement for  $e^+e^- \rightarrow \pi^+\pi^-$  [32] mentioned above.

<sup>3</sup>With  $\tau$  data for the two-pion contribution, together with the estimate for the required isospin-breaking corrections obtained from the model of Ref. [37], this discrepancy is reduced [38].

Smaller charm- and bottom-quark contributions (both connected and disconnected) are also included. Electromagnetic (EM) and strong-isospin-breaking (SIB) corrections are treated perturbatively to first order in the fine-structure constant  $\alpha$  and the up-down quark-mass difference, which is sufficient for the present precision. The data-driven approach, in turn, is based on the analysis of exclusive hadronic electroproduction data, channel by channel, up to squared hadronic invariant masses,  $s$ , of about  $4 \text{ GeV}^2$ , and inclusive data and/or perturbative QCD (pQCD) at higher  $s$ .

Several lattice collaborations have produced partial results for the different contributions to  $a_\mu^{\text{HVP}}$  using the RBC/UKQCD and other windows. For the intermediate window, ten recent, mutually compatible, lattice-QCD results for the isospin-symmetric light-quark connected (lqc) component now exist [30, 33, 39–46]. Results for the lqc short-distance contribution have also been obtained by six independent groups [33, 43, 45–48] and, recently, two results for the lqc contribution to the long-distance window have been published [49, 50]. Other sub-dominant contributions, such as the full strange-quark and light-quark disconnected contributions have also been calculated by different lattice-QCD collaborations [30, 33, 34, 43–45, 47, 51–53].

In order to sharpen the comparison of the data-driven and lattice-QCD approaches to  $a_\mu^{\text{HVP}}$  it is highly desirable to have data-driven estimates of the different components of the lattice results. In recent papers [54–57], we have shown that it is possible to reorganize the data-driven computation of  $a_\mu^{\text{HVP}}$  to reliably estimate the lqc, as well as the complete strange-quark plus light-quark disconnected (s+lqd), contributions to  $a_\mu^{\text{HVP}}$ . We demonstrated that the discrepancy with pre-CMD-3 data-driven results [12, 13] originates mostly in the intermediate window isospin-symmetric lqc contribution [56] while s+lqd data-driven results are in good agreement with their lattice counterparts [57]. In the present paper, we obtain the data-driven determinations of the lqc and s+lqd components of the short- and long-distance isospin-symmetric RBC/UKQCD windows. We present results based on the pre-CMD-3 data combination of Ref. [13], referred to as the “KNT19 data,” but estimate, as well, the potential impact of the new CMD-3 results for the  $\pi^+\pi^-$  electroproduction cross sections. We emphasize that this latter study, using CMD-3 data, represents only a first exploration, since, given the present discrepancies in the  $2\pi$  cross-section data-base, a meaningful combination of all experimental  $2\pi$  data appears impossible. This paper concludes our data-driven determinations of the lqc and s+lqd contributions to the RBC/UKQCD windows and provides additional benchmarks for the comparison with present and future lattice-QCD results.

The paper is organized as follows. In Sec. 2, we define the RBC/UKQCD windows that are studied in this paper and briefly review the strategy for the data-driven determination of the lqc and s+lqd contributions to  $a_\mu^{\text{HVP}}$  and the intermediate RBC/UKQCD window already employed in Refs. [54–57]. In Sec. 3, we discuss the implementation of this strategy for the short-distance (SD) and long-distance (LD) windows and give intermediate results for the different contributions to the lqc and s+lqd components of the windows. In Sec. 4, we present our final, pre-CMD-3 data-based results for the SD and LD windows, quoting, for completeness, also the results for the intermediate window and the total HVP contribution, already presented in Refs. [54–57]. In Sec. 5 we make an exploratory study of the potential impact of the CMD-3 results for the  $2\pi$  channel. Our conclusions are presented in Sec. 6.

## 2 Review of the general strategy

Here, we present a concise review of the strategy employed in this paper. It has been described in detail in our previous publications [54–57] to which we refer for additional details.

### 2.1 Windows

We start by defining the window quantities considered in this paper. The master formula for the data-driven (or dispersive) approach to the leading order  $a_\mu^{\text{HVP}}$  is [58–60]

$$a_\mu^{\text{HVP}} = \frac{4\alpha^2 m_\mu^2}{3} \int_{m_\pi^2}^{\infty} ds \frac{\hat{K}(s)}{s^2} \rho_{\text{EM}}(s), \quad (1)$$

where  $m_\pi$  is the neutral pion mass and  $\rho_{\text{EM}}(s)$  represents the inclusive EM-current hadronic spectral function, which is related to the  $R$  ratio derived from the bare inclusive hadronic electroproduction cross section,  $\sigma^{(0)}[e^+e^- \rightarrow \text{hadrons}(+\gamma)]$ , by

$$\begin{aligned} \rho_{\text{EM}}(s) &= \frac{1}{12\pi^2} R(s), \\ R(s) &= \frac{3s}{4\pi\alpha} \sigma^{(0)}[e^+e^- \rightarrow \text{hadrons}(+\gamma)], \end{aligned} \quad (2)$$

where the kernel  $\hat{K}(s)$  is a smoothly varying, monotonically increasing function with  $\hat{K}(4m_\pi^2) \approx 0.63$  at the two-pion threshold and  $\lim_{s \rightarrow \infty} \hat{K}(s) = 1$ .<sup>4</sup> In terms of the so-called time-momentum representation,  $a_\mu^{\text{HVP}}$  can be obtained from the Euclidean-time two-point correlator [61]

$$C(t) = \frac{1}{3} \sum_{i=1}^3 \int d^3x \langle j_i^{\text{EM}}(\vec{x}, t) j_i^{\text{EM}}(0) \rangle = \frac{1}{2} \int_{m_\pi^2}^{\infty} ds \sqrt{s} e^{-\sqrt{s}t} \rho_{\text{EM}}(s) \quad (t > 0), \quad (3)$$

built from the EM current  $j_i^{\text{EM}}(\vec{x}, t)$  as

$$a_\mu^{\text{HVP}} = 2 \int_0^\infty dt w(t) C(t), \quad (4)$$

where the function  $w(t)$  is known and can be obtained from  $\hat{K}(s)$ .<sup>5</sup>

The windowed versions (“windows” in what follows) we consider in this work, originally introduced in Ref. [34], are the SD, intermediate (int), and LD windows obtained by inserting the functions

$$\begin{aligned} W_{\text{SD}}(t) &= 1 - \Theta(t, t_0, \Delta), \\ W_{\text{int}}(t) &= \Theta(t, t_0, \Delta) - \Theta(t, t_1, \Delta), \\ W_{\text{LD}}(t) &= \Theta(t, t_1, \Delta), \end{aligned} \quad (5)$$

respectively, with

$$\Theta(t, t', \Delta) = \frac{1}{2} \left( 1 + \tanh \frac{t - t'}{\Delta} \right) \quad (6)$$

<sup>4</sup>For the explicit expressions, we refer to e.g. Ref. [5].

<sup>5</sup>For explicit expressions and a useful approximation see Refs. [61, 62].

and  $t_0 = 0.4 \text{ fm}$ ,  $t_1 = 1.0 \text{ fm}$ , and  $\Delta = 0.15 \text{ fm}$ , into the representation of Eq. (4), leading to

$$\begin{aligned} a_\mu^{\text{win}} &= 2 \int_0^\infty dt W_{\text{win}}(t) w(t) C(t) \\ &= \frac{4\alpha^2 m_\mu^2}{3} \int_{m_\pi^2}^\infty ds \frac{\hat{K}(s)}{s^2} \widetilde{W}_{\text{win}}(s) \rho_{\text{EM}}(s), \end{aligned} \quad (7)$$

where  $\text{win} = \{\text{SD}, \text{int}, \text{LD}\}$  and the window function in  $s$ -space is written as

$$\widetilde{W}_{\text{win}}(s) = \frac{\int_0^\infty dt W_{\text{win}}(t) w(t) e^{-\sqrt{s}t}}{\int_0^\infty dt w(t) e^{-\sqrt{s}t}}. \quad (8)$$

By construction,  $a_\mu^{\text{HVP}}$  is given by the sum of the three windows defined above.

## 2.2 Light-quark connected and strange plus disconnected spectral functions in the isospin limit

Our data-driven determination of the lqc and the s+lqd contributions to  $a_\mu^{\text{HVP}}$  follows the strategy implemented for the first time in Refs. [54, 55]. We start from the decomposition of the three-light-flavor EM current into its  $I = 1$  (flavor octet label 3) and  $I = 0$  (flavor octet label 8) parts, and the related decompositions of  $\rho_{\text{EM}}(s)$ ,  $C(t)$  and any weighted integrals thereof, into their pure  $I = 1/0$  (flavor octet labels 33/88) and mixed-isospin (MI, flavor octet labels 38) components. In the isospin limit, the pure  $I = 1$  contributions are entirely light-quark connected and the corresponding pure  $I = 0$  lqc contributions exactly  $1/9$  times their  $I = 1$  lqc counterparts. Thus, for example, the total lqc contribution to the EM spectral function is

$$\rho_{\text{EM}}^{\text{lqc}}(s) = \frac{10}{9} \rho_{\text{EM}}^{I=1}(s), \quad (9)$$

and one can obtain the full strange plus light-quark disconnected contribution from the combination

$$\begin{aligned} \rho_{\text{EM}}^{\text{s+lqd}}(s) &= \rho_{\text{EM}}^{I=0}(s) - \frac{1}{9} \rho_{\text{EM}}^{I=1}(s) \\ &= \rho_{\text{EM}}(s) - \frac{10}{9} \rho_{\text{EM}}^{I=1}(s). \end{aligned} \quad (10)$$

Our main task is, hence, the identification, with sufficient precision, of the  $I = 1$  and  $I = 0$  components of  $\rho_{\text{EM}}$  and any associated weighted integral quantities. As outlined below, this can be accomplished on a channel-by-channel basis, using isospin symmetry, in the exclusive-mode region of the  $R(s)$  data. In this work, we employ the results for the exclusive-mode components of the pre-CMD-3  $R(s)$  data combination of Ref. [13], commonly referred to as ‘KNT19.’ It would be interesting to perform our analysis using other data combinations, such as that of Ref. [12], but this would require access to their exclusive spectra, channel-by-channel and with all correlations, which, to the best of our knowledge, is not publicly available.

Substituting the spectral functions for the lqc and s+lqd components, Eq. (9) and Eq. (10), respectively, into Eq. (7), one obtains the respective isospin-limit contributions to each of the  $a_\mu^{\text{HVP}}$  windows, which we denote by  $a_\mu^{\text{win,lqc}}$  and  $a_\mu^{\text{win,s+lqd}}$ .

### 3 Implementation and intermediate results

Four different ingredients are required for our determinations of the isospin-symmetric lqc and s+lqd components,  $a_\mu^{\text{win,lqc}}$  and  $a_\mu^{\text{win,s+lqd}}$ , of the RBC/UKQCD windows defined in Eqs. (5) to (7). The first is the set of contributions from exclusive modes which are  $G$ -parity eigenstates, where the  $G$ -parity allows the isospin of the contribution to be unambiguously identified. We refer to such modes generically as “unambiguous.” The sum of  $G$ -parity-positive-mode contributions dominates the lqc component of the three windows. We discuss the unambiguous-mode contributions in Sec. 3.1. The second ingredient is the set of  $I = 0$  and 1 components of contributions from exclusive modes that are not  $G$ -parity eigenstates, which we refer to as “ambiguous.” The isospin separation for such ambiguous-mode contributions is discussed in Sec. 3.2. For the KNT19 compilation, the “exclusive-mode region” (the region of squared hadronic invariant masses,  $s$ , in which  $R(s)$  is saturated by the sum of measured exclusive-mode contributions) extends up to  $s = (1.937 \text{ GeV})^2$ . We refer to the region above this as the “inclusive region.” The third ingredient is the set of inclusive-region contributions. For these we employ (pQCD), supplemented with an estimate for the impact of quark-hadron duality violation, as explained in Sec. 3.3. The fourth ingredient, discussed in Sec. 3.4, is the EM and SIB corrections that must be applied before performing comparisons with isospin-symmetric lattice-QCD results.

#### 3.1 Modes with unambiguous isospin

As discussed in detail in Refs. [54–57], in the isospin limit, modes with positive (negative)  $G$ -parity have isospin  $I = 1$  ( $I = 0$ ). In Tabs. 1 and 2, we give the contributions of each of the  $G$ -parity unambiguous modes  $X$  present in the KNT19 data combination to the three windows of Eq. (5), denoted  $[a_\mu^{\text{win}}]_X$ , as well as to the total HVP contribution,  $[a_\mu^{\text{HVP}}]_X$ .<sup>6</sup> Although the central value for  $[a_\mu^{\text{HVP}}]_X$  is always the sum of the central values of the contributions to the three windows from the same mode, the uncertainty in the fifth column of Tabs. 1 and 2 includes the effect of correlations among the errors on the three associated window quantities. The results for the intermediate window and for the total HVP were already given in Refs. [54, 56] and are repeated here for completeness.

The corresponding exclusive-mode contributions to the full lqc window totals are obtained by multiplying the entries in Tab. 1 by 10/9, as per Eq. (9). The resulting sums of lqc contributions from all unambiguous modes are listed in Tab. 5. The contributions of the unambiguous modes to the s+lqd components are given by the combination shown in Eq. (10); the totals of these contributions for each window appear in Tab. 6.

#### 3.2 Modes with ambiguous isospin

We turn now to the modes with no definite isospin. These are of two distinct types, those for which external information can be used to help separate the different isospin components and those for which this is not possible. Fortunately such external information is available for the channels,  $K\bar{K}$ ,  $K\bar{K}\pi$  and  $\pi^0/\eta + \gamma$ , which give the

---

<sup>6</sup>Entries whose mode names include the phrase “low- $s$ ” are those labelling very-near-threshold contributions for which the underlying  $R(s)$  contributions were obtained using Chiral Perturbation Theory in the KNT19 exclusive-mode compilation.

Table 1: Contributions from  $G$ -parity positive modes (hence  $I = 1$ ) to  $a_\mu^{\text{SD}}$ ,  $a_\mu^{\text{int}}$ ,  $a_\mu^{\text{LD}}$ , and  $a_\mu^{\text{tot}}$  for  $\sqrt{s} \leq 1.937$  GeV obtained from KNT19 [13] exclusive-mode spectra. The label “npp” stands for “non-purely pionic.” All entries in units of  $10^{-10}$ . Uncertainties in the last column take into account the correlations between the three windows.

$I = 1$ modes $X$	$[a_\mu^{\text{SD}}]_X \times 10^{10}$	$[a_\mu^{\text{int}}]_X \times 10^{10}$	$[a_\mu^{\text{LD}}]_X \times 10^{10}$	$[a_\mu^{\text{HVP}}]_X \times 10^{10}$
low- $s$ $\pi^+\pi^-$	0.0010(00)	0.02(00)	0.842(18)	0.867(18)
$\pi^+\pi^-$	14.927(52)	144.13(49)	344.4(1.4)	503.5(1.9)
$2\pi^+2\pi^-$	3.239(43)	9.29(13)	2.334(34)	14.87(20)
$\pi^+\pi^-2\pi^0$	3.98(16)	11.94(48)	3.46(14)	19.39(78)
$3\pi^+3\pi^-$ (no $\omega$ )	0.0746(47)	0.14(01)	0.01485(95)	0.231(15)
$2\pi^+2\pi^-2\pi^0$ (no $\eta$ )	0.426(52)	0.83(11)	0.092(13)	1.35(17)
$\pi^+\pi^-4\pi^0$ (no $\eta$ )	0.067(67)	0.13(13)	0.014(14)	0.21(21)
$\eta\pi^+\pi^-$	0.333(12)	0.85(03)	0.1594(63)	1.340(50)
$\eta2\pi^+2\pi^-$	0.0239(33)	0.05(01)	0.00547(98)	0.076(11)
$\eta\pi^+\pi^-2\pi^0$	0.0407(66)	0.07(01)	0.0065(11)	0.119(20)
$\omega(\rightarrow \pi^0\gamma)\pi^0$	0.1469(34)	0.53(01)	0.2014(42)	0.882(19)
$\omega(\rightarrow \text{npp})3\pi$	0.0529(99)	0.10(02)	0.0116(23)	0.168(32)
$\omega\eta\pi^0$	0.081(18)	0.15(03)	0.0144(29)	0.242(53)
Total ( $I = 1$ )	23.40(19)	168.24(72)	351.6(1.4)	543.2(2.1)

largest of the ambiguous-mode contributions. Contributions from other ambiguous modes all turn out to be small. The strategy used to perform the ambiguous-mode isospin separations is described in Ref. [57] (see also Ref. [54]) and reviewed briefly below.

We start from those ambiguous modes having only  $I = 0$  and  $I = 1$  contributions in the isospin limit and for which no external information is available. The small contributions from these modes are treated using a “maximally conservative” prescription, based on the observation that, because of spectral positivity, the  $I = 0$  and  $I = 1$  parts of the contribution from the given mode  $X$  must both lie between 0 and the full experimental  $I = 1 + 0$  total obtained from the KNT19  $R(s)$  data. The  $I = 0$  and  $I = 1$  components are then guaranteed to lie, respectively, in the ranges  $(50 \pm 50)\%$  and  $(50 \mp 50)\%$  times the  $I = 0 + 1$  total, with the two errors 100% anticorrelated. The lqc and the s+lqd parts of the mode- $X$  contribution to the EM spectral function then lie in the following ranges [54]

$$\begin{aligned}
 [\rho_{\text{EM}}^{\text{lqc}}]_X &= \left(\frac{5}{9} \pm \frac{5}{9}\right) [\rho_{\text{EM}}]_X, \\
 [\rho_{\text{EM}}^{\text{s+lqd}}]_X &= \left(\frac{4}{9} \pm \frac{5}{9}\right) [\rho_{\text{EM}}]_X.
 \end{aligned} \tag{11}$$

This maximally conservative separation of  $[\rho_{\text{EM}}]_X$  produces related results for the contributions to the window quantities  $[a_\mu^{\text{win,lqc}}]_X$  and  $[a_\mu^{\text{win,s+lqd}}]_X$  when used in Eq. (7).



Table 2: Contributions from  $G$ -parity negative modes (hence  $I = 0$ ) to  $a_\mu^{\text{SD}}$ ,  $a_\mu^{\text{int}}$ ,  $a_\mu^{\text{LD}}$ , and  $a_\mu^{\text{HVP}}$  for  $\sqrt{s} \leq 1.937$  GeV obtained from KNT19 [13] exclusive-mode spectra. The label “npp” stands for “non-purely pionic.” Uncertainties in the last column take into account the correlations between the three windows. All entries in units of  $10^{-10}$ .

$I = 0$ modes $X$	$[a_\mu^{\text{int}}]_X \times 10^{10}$	$[a_\mu^{\text{SD}}]_X \times 10^{10}$	$[a_\mu^{\text{LD}}]_X \times 10^{10}$	$[a_\mu^{\text{tot}}]_X \times 10^{10}$
low- $s$ $3\pi$	0.0003	0.003	0.01	0.014
$3\pi$	2.609(46)	18.69(35)	25.42(54)	46.73(94)
$2\pi^+2\pi^-\pi^0$ (no $\omega$ , $\eta$ )	0.266(24)	0.613(57)	0.100(10)	0.979(90)
$\pi^+\pi^-3\pi^0$ (no $\eta$ )	0.172(30)	0.388(72)	0.059(12)	0.62(11)
$3\pi^+3\pi^-\pi^0$ (no $\omega$ , $\eta$ )	-0.0010(17)	-0.0027(32)	-0.00053(35)	-0.0043(53)
$\eta\pi^+\pi^-\pi^0$ (no $\omega$ )	0.209(23)	0.441(51)	0.0566(72)	0.706(81)
$\eta\omega$	0.0823(62)	0.187(14)	0.0267(20)	0.296(22)
$\omega(\rightarrow \text{npp})2\pi$	0.0370(40)	0.0836(92)	0.0124(14)	0.133(15)
$\omega 2\pi^+2\pi^-$	0.00246(69)	0.0045(13)	0.00044(13)	0.0074(21)
$\eta\phi$	0.1225(57)	0.253(0.012)	0.0304(15)	0.406(19)
$\phi \rightarrow (\text{unaccounted})$	0.0036(36)	0.02(0.02)	0.017(17)	0.043(43)
Total ( $I = 0$ )	3.502(65)	20.69(37)	25.74(54)	49.93(95)

It is crucial, however, to have better control over the dominant contributions from ambiguous modes than would be provided by the maximally conservative treatment, especially those arising from the  $K\bar{K}$  and, to a lesser extent, the  $K\bar{K}\pi$  channels. For these channels, external experimental information can be used to assess the  $I = 1$  component of the total  $I = 1 + 0$  sum. For the  $K\bar{K}$  modes ( $K^+K^-$  and  $K^0\bar{K}^0$ ), this external information comes in the form of BaBar’s measurement of the differential decay distribution of  $\tau \rightarrow K^-K^0\nu_\tau$  [63], which provides a determination of the  $K\bar{K}$  contribution to the charged-current  $I = 1$  vector spectral function, which in turn, via the conserved vector current (CVC) relation, provides a determination of the  $I = 1$  part of the  $K\bar{K}$  contribution to  $\rho_{EM}(s)$ , and hence<sup>7</sup> an estimate of the  $I = 1$  part of the  $K\bar{K}$  contribution to the various window integrals in the region up to the endpoint,  $s = 2.7556$  GeV<sup>2</sup>, of the BaBar  $\tau$  data. Above this point, we integrate the  $I = 1 + 0$  tail of the KNT19  $K\bar{K}$  spectrum, applying the maximally conservative separation to this small remainder to obtain our final  $I = 1$  and  $I = 0$  totals for the full exclusive-region  $K\bar{K}$  contributions. As an example, for the lqc contribution to the LD window, this procedure gives, using Eq. (9),

$$[a_\mu^{\text{LD}}]_{K\bar{K}}^{\text{lqc}} = \frac{10}{9}(0.1743(84) + 0.0065(65)) \times 10^{-10} = 0.201(12) \times 10^{-10}, \quad (12)$$

where the first number in parenthesis is the  $I = 1$  contribution obtained using BaBar  $\tau \rightarrow K^-K^0\nu_\tau$  data and the second is the contribution from the tail of the KNT19

<sup>7</sup>For our purposes, isospin-breaking corrections to the CVC relation can safely be neglected. In the case of Eq. (12), e.g., a 1% isospin-breaking correction would amount to  $0.002 \times 10^{-10}$ , which can very safely be neglected when compared with other uncertainties entering this determination.



Table 3: Contributions of modes with no definite isospin to the lqc parts of  $a_\mu^{\text{SD}}$ ,  $a_\mu^{\text{int}}$ ,  $a_\mu^{\text{LD}}$ , and  $a_\mu^{\text{HVP}}$ . See the text for the details of the treatment of each channel. The label “npp” stands for “non-purely pionic.” Uncertainties in the last column take into account the correlations between the three windows. All entries in units of  $10^{-10}$ .

mode	$[a_\mu^{\text{SD}}]_X^{\text{lqc}} \times 10^{10}$	$[a_\mu^{\text{int}}]_X^{\text{lqc}} \times 10^{10}$	$[a_\mu^{\text{LD}}]_X^{\text{lqc}} \times 10^{10}$	$[a_\mu^{\text{tot}}]_X^{\text{lqc}} \times 10^{10}$
$K\bar{K}$	0.167(30)	0.579(64)	0.201(12)	0.95(10)
$K\bar{K}\pi$	0.219(36)	0.521(86)	0.083(14)	0.82(14)
$\pi^0\gamma + \eta\gamma$	0.0165(15)	0.137(13)	0.204(21)	0.36(4)
$K\bar{K}2\pi$	0.32(32)	0.60(60)	0.062(62)	0.98(98)
$K\bar{K}3\pi$	0.0082(82)	0.012(12)	0.00054(54)	0.21(21)
low- $s$ $\pi^0\gamma + \eta\gamma$	0.00054(54)	0.0082(82)	0.061(61)	0.070(70)
$N\bar{N}$	0.012(12)	0.019(19)	0.0015(15)	0.033(33)
$\eta(\rightarrow \text{npp})K\bar{K}(\text{no } \phi)$	0.0027(27)	0.0050(50)	0.00052(52)	0.0082(82)
$\omega(\rightarrow \text{npp})K\bar{K}$	0.00085(85)	0.0012(12)	0.000056(56)	0.0021(21)
Total (lqc)	0.75(32)	1.88(61)	0.613(91)	3.2(1.0)

spectrum, evaluated using the maximally conservative separation of Eq. (11). Results for the other windows are given in the second row of Tab. 3. The s+lqd LD window  $K\bar{K}$  contribution is, similarly, using Eq. (10),

$$[a_\mu^{\text{LD}}]_{K\bar{K}}^{\text{s+lqd}} = \left[ 13.37(11) - \frac{1}{9} \times 0.181(11) \right] \times 10^{-10} = 13.35(11) \times 10^{-10},$$

where the first number in square brackets is the  $I = 0$  total and the second number (one-ninth of) the  $I = 1$  part. The dominance of the  $I = 0$  component is a result of the enhancement produced by the  $\phi$  resonance. The analogous results for the other windows are given in the first row of Tab. 4.

For the  $K\bar{K}\pi$  contributions, the needed external information is provided by BaBar’s Dalitz plot separation of the  $I = 1$  and  $I = 0$  parts of the  $K\bar{K}\pi$  cross sections [64]. The BaBar  $I = 1$  cross sections provide a determination of the  $I = 1$  part of the  $K\bar{K}\pi$  contribution to  $\rho_{EM}(s)$ , and hence of the  $K\bar{K}\pi$  mode contributions to the lqc window quantities. The corresponding  $I = 0$  contributions are obtained by subtracting the BaBar-based  $I = 1$  results from the KNT19  $I = 1 + 0$  totals. As an example, we find, for the  $K\bar{K}\pi$  contribution to the lqc component of the LD window, the result

$$[a_\mu^{\text{LD}}]_{K\bar{K}\pi}^{\text{lqc}} = \frac{10}{9} [a_\mu^{\text{LD}}]_{K\bar{K}\pi}^{I=1} = 0.083(14) \times 10^{-10}. \quad (13)$$

The corresponding results for the other windows are given in Tab. 3. Similarly, for the  $K\bar{K}\pi$  contribution to the s+lqd component of the LD window, we find, using the second line of Eq. (10),

$$\begin{aligned} [a_\mu^{\text{LD}}]_{K\bar{K}\pi}^{\text{s+lqd}} &= [a_\mu^{\text{LD}}]_{K\bar{K}\pi} - \frac{10}{9} [a_\mu^{\text{LD}}]_{K\bar{K}\pi}^{I=1} \\ &= [0.263(11) - \frac{10}{9} \times 0.075(13)] \times 10^{-10} = 0.180(18) \times 10^{-10}, \end{aligned} \quad (14)$$

with the results for the other windows given in Tab. 4.

For the  $K\bar{K}2\pi$  channel, a modest in-principle improvement can be achieved over the purely maximally conservative separation treatment by first using BaBar’s measurement of the  $e^+e^- \rightarrow \phi\pi\pi$  cross sections [65] and the PDG  $\phi \rightarrow K\bar{K}$  branching fraction to quantify the purely  $I = 0$   $e^+e^- \rightarrow \phi(\rightarrow K\bar{K})\pi\pi$  contribution and then applying the maximally conservative separation treatment to the rest of the  $K\bar{K}2\pi$  contributions. In practice, the improvement is too small to make a significant impact and the final uncertainties on the  $K\bar{K}2\pi$  contributions are still of the order of 100%, as can be seen in Tabs. 3 and 4.

Finally, for the radiative modes  $\pi^0\gamma$  and  $\eta\gamma$ , a full decomposition into pure  $I = 1$ , pure  $I = 0$  and MI components turns out to be possible owing to the strong dominance of the observed exclusive-mode-region cross sections by intermediate vector meson contributions. We briefly outline the decomposition procedure below, referring the reader to App. B of Ref. [57] for further details. We note first that the measured  $e^+e^- \rightarrow \pi^0\gamma$  and  $e^+e^- \rightarrow \eta\gamma$  cross sections display prominent narrow  $\omega$  and  $\phi$  resonance peaks. The normalizations of the underlying  $V = \omega$  and  $\phi$  contributions to the amplitudes are, of course, set by the measured  $V \rightarrow e^+e^-$  and  $V \rightarrow P\gamma$  ( $P = \pi, \eta$ ) widths. Less immediately evident visually, but necessarily also present, are broad  $\rho$  contributions, with normalizations set by the measured  $\rho \rightarrow e^+e^-$  and  $\rho \rightarrow P\gamma$  widths. In Ref. [57] it was shown that, using PDG input for the above widths, the VMD representations of the  $e^+e^- \rightarrow P\gamma$  amplitudes produced by summing over the resulting externally determined  $V = \rho, \omega$  and  $\phi$  contributions accurately reproduce the observed cross sections and, not surprisingly therefore, provide accurate representation of the resulting full HVP and intermediate window integrals. Neglecting additional IB effects in the photon-vector-meson couplings (since the  $e^+e^- \rightarrow \pi^0\gamma$  and  $e^+e^- \rightarrow \eta\gamma$  cross sections and associated weighted integrals are already  $O(\alpha_{EM})$  and hence first order in IB), the  $\rho$  contributions to the two amplitudes come solely from the coupling of the  $\rho$  to the  $I = 1$  (flavor 3) part of the EM current, and the  $\omega$  and  $\phi$  contributions solely from the couplings of the  $\omega$  and  $\phi$  to the  $I = 0$  (flavor 8) part. Thus, to first order in IB, the pure  $I = 1$  (flavor 33) parts of the cross sections come from the squared modulus of the  $\rho$  contribution to the amplitude in question, the pure  $I = 0$  (flavor 88) part from the squared modulus of the sum of the  $\omega$  and  $\phi$  contributions, and the MI (flavor 38) part from the interference between the  $\rho$  and  $\omega + \phi$  contributions. The  $\pi^0\gamma$  and  $\eta\gamma$  contributions to the lqc and s+lqd components of the SD and LD windows produced by the resulting  $I = 1/I = 0$ /MI decompositions are listed in Tabs. 3 and 4, where, for completeness, we also list the corresponding HVP and intermediate window results, reported previously in Ref. [57].

The small contributions from the remaining ambiguous exclusive modes of the KNT19 data compilation, are handled using the maximally conservative separation treatment, and the results, again, collected in Tabs. 3 and 4.

### 3.3 Perturbative contribution above $s = (1.937 \text{ GeV})^2$

In the inclusive region, i.e., for hadronic squared invariant masses  $s > (1.937 \text{ GeV})^2$ , we use massless three-flavor pQCD (we have checked that strange-quark mass corrections can safely be neglected [54]). The Adler function is exactly known up to  $\mathcal{O}(\alpha_s^4)$  [66] and we supplement it with an estimate for the  $\mathcal{O}(\alpha_s^5)$  coefficient, as described in our previous

Table 4: Contributions of modes with no definite isospin to the s+lqcd parts of  $a_\mu^{\text{SD}}$ ,  $a_\mu^{\text{int}}$ ,  $a_\mu^{\text{LD}}$ , and  $a_\mu^{\text{HVP}}$ . See text for the details of the treatment of each channel. The label “npp” stands for “non-purely pionic.” Uncertainties in the last column take into account the correlations between the three windows. All entries in units of  $10^{-10}$ .

mode	$[a_\mu^{\text{SD}}]_X^{\text{s+lqcd}} \times 10^{10}$	$[a_\mu^{\text{int}}]_X^{\text{s+lqcd}} \times 10^{10}$	$[a_\mu^{\text{LD}}]_X^{\text{s+lqcd}} \times 10^{10}$	$[a_\mu^{\text{tot}}]_X^{\text{s+lqcd}} \times 10^{10}$
$K\bar{K}$	3.229(39)	18.55(17)	13.35(11)	35.13(31)
$K\bar{K}\pi$	0.518(48)	1.19(11)	0.180(18)	1.89(18)
$\pi^0\gamma + \eta\gamma$	0.1763(66)	1.50(6)	2.32(10)	4.00(17)
$K\bar{K}2\pi$	0.30(32)	0.58(60)	0.062(62)	0.94(98)
$K\bar{K}3\pi$	0.0065(82)	0.009(12)	0.00043(54)	0.016(20)
low-s $\pi^0\gamma + \eta\gamma$	0.00043(54)	0.0066(82)	0.049(61)	0.056(70)
$N\bar{N}$	0.010(12)	0.016(19)	0.0012(15)	0.026(33)
$\eta(\rightarrow \text{npp})K\bar{K}(\text{no } \phi)$	0.0021(27)	0.0040(50)	0.00042(52)	0.0065(82)
$\omega(\rightarrow \text{npp})K\bar{K}$	0.00068(85)	0.0010(12)	0.000045(56)	0.0017(21)
Total (s+lqcd)	4.25(33)	21.86(64)	15.96(18)	42.1(1.1)

works [54,55,57]. To this perturbative result, we add an estimate of the duality violating (DV) contribution, which, essentially, captures the residual oscillations in the spectral function due the tails of the higher-mass resonances. To parametrize the DVs, we employ results from our previous study of the  $I = 1$  spectral function in  $\tau \rightarrow \text{hadrons} + \nu_\tau$  [67] decays as well as knowledge about the  $I = 0$  contribution from  $e^+e^- \rightarrow \text{hadrons}$  [68].

Perturbative QCD is in good agreement with inclusive  $R(s)$  data from BES [69,70] and KEDR [71] for  $s \geq 4 \text{ GeV}^2$ , but in some tension with recent, more precise results from BES-III [72] below charm threshold. Because of this tension, and since the DV contribution represents an essential limitation of perturbation theory, we have significantly enlarged the error associated with the use of pQCD in the inclusive region — which is typically assessed using estimates of the size of missing higher-orders in the  $\alpha_s$  expansion. We consider, therefore, as our final error on the inclusive-region contribution the central value of the DV component. This procedure produces a significantly increased error on the inclusive-region contributions to the lqc and s+lqcd components. For the lqc case, the error is enlarged by factors that vary between 3 and 11 (depending on the window) while for the s+lqcd component the enlargement can be up to factors of order 30. As we show here, because of the small contribution from the inclusive region in essentially all cases (the exception is the SD window, as could be expected) this increase in error in the perturbative contribution has no meaningful impact on the precision of our final results.

Since the details of our perturbative description in the inclusive region, as well as of the parametrization of the DVs that we employ, have already been extensively discussed in Ref. [54,57] we, here, simply quote the final numbers for the pQCD+DV contributions in Tabs. 5 and 6.

### 3.4 Isospin-breaking corrections

The final step is to estimate electromagnetic (EM) and strong-isospin-breaking (SIB) contributions to the results discussed above. These contributions must be subtracted

before comparing our results with those of isospin-symmetric lattice QCD. We follow the treatment discussed extensively in our previous works [54, 55, 57] and here simply summarize the application of this framework to the SD and LD windows. Our isospin-symmetric results, as is the case for many lattice groups, correspond to a definition of the isospin limit of QCD in which all pions have the neutral pion mass.

We work to first order in IB and start from the observation that, to this precision, SIB appears only in the MI component of  $\rho_{\text{EM}}(s)$  while EM contributions appear in all of the pure  $I = 1$ , pure  $I = 0$  and MI components. MI contributions, in general, produce small IB “contaminations” of the nominally pure  $I = 1$   $G$ -parity positive and nominally pure  $I = 0$   $G$ -parity negative exclusive-mode contributions discussed above. These must be subtracted, mode-by-mode, to arrive at data-driven isospin-limit lqc and s+lqc results suitable for comparison to the corresponding lattice results. It is expected, however, that the dominant such contaminations will be those in the  $2\pi$  and  $3\pi$  channels, which are strongly enhanced by the effects of  $\rho - \omega$  mixing through the processes  $e^+e^- \rightarrow \omega \rightarrow \rho \rightarrow 2\pi$  and  $e^+e^- \rightarrow \rho \rightarrow \omega \rightarrow 3\pi$ . To estimate the resulting dominant MI contaminations we use the results of Ref. [73–75] where the  $2\pi$  and  $3\pi$  electroproduction data were fitted with dispersive representations incorporating the effects of  $\rho - \omega$  mixing. Since these estimates are obtained using experimental input, they, of course, include both the EM and SIB components of the MI contributions.

The resulting estimates for the MI components of the nominally  $I = 1$   $2\pi$ -mode contributions to HVP integral and the three windows discussed in this paper can be found in Tab. I of Ref. [73] and read

$$\begin{aligned} [a_\mu^{\text{SD}}]_{\pi\pi}^{\text{MI}} \times 10^{10} &= 0.06(1), \\ [a_\mu^{\text{int}}]_{\pi\pi}^{\text{MI}} \times 10^{10} &= 0.86(6), \\ [a_\mu^{\text{LD}}]_{\pi\pi}^{\text{MI}} \times 10^{10} &= 2.87(12), \\ [a_\mu^{\text{HVP}}]_{\pi\pi}^{\text{MI}} \times 10^{10} &= 3.79(19). \end{aligned} \tag{15}$$

In the  $2\pi$  channel, this MI contribution, in spite of the enhancement due to the  $\rho - \omega$  mixing, never exceeds 0.85% of the  $2\pi$  total given in Tab. 1. With no analogous narrow, nearby resonance enhancements of this type expected for other nominally  $I = 1$  modes, we consider it safe to assume that the total MI contamination present in the contributions from these other modes will not exceed 1% of the sum of their contributions. In this spirit, we add to the results of Eq. (15) an additional uncertainty equal to 1% of the sum of all non- $2\pi$  nominally  $I = 1$  contributions, from both unambiguous and ambiguous modes (the latter with the exception of the radiative modes,  $\pi^0\gamma$  and  $\eta\gamma$ , where the VMD representation provides a full  $I = 1/I = 0$ /MI separation and there is, thus, no MI contamination of either the  $I = 1$  or  $I = 0$  contribution). The non- $2\pi$ ,  $I = 1$  totals for each window, obtained by adding to the unambiguous-mode  $I = 1$  results of Tab. 1 the  $I = 1$  components of the ambiguous-mode contributions that can be inferred from Tab. 3 (excluding the radiative channels  $\pi^0\gamma$  and  $\eta\gamma$ ), are the following

$$\begin{aligned} [a_\mu^{\text{SD}}]_{\text{non-}2\pi}^{I=1} \times 10^{10} &= 9.12(34), \\ [a_\mu^{\text{int}}]_{\text{non-}2\pi}^{I=1} \times 10^{10} &= 25.66(76), \\ [a_\mu^{\text{LD}}]_{\text{non-}2\pi}^{I=1} \times 10^{10} &= 6.68(17), \\ [a_\mu^{\text{tot}}]_{\text{non-}2\pi}^{I=1} \times 10^{10} &= 41.5(1.2). \end{aligned} \tag{16}$$

Our final estimates for the nominally  $I = 1$  MI contaminations consist of the numbers given in Eq. (15) with 1% of the central values of Eq. (16) added in quadrature as an additional uncertainty. These results are to be multiplied by 10/9 to convert them to the corresponding lqc MI contaminations and subtracted from the sum of the uncorrected lqc results obtained above, shown in the first three lines of Tab. 5. The resulting MI corrections, to be added to the other entries, are listed in line four of this table.

The procedure employed to estimate the  $I = 0$  MI IB contribution is very similar: we use the results of Ref. [73] as estimates of the MI contaminations,  $[a_\mu^{\text{win}}]_{3\pi}^{\text{MI}}$ , present in the nominally  $I = 0$   $3\pi$  window contributions and add to those results an additional uncertainty of 1% of the total of all non- $3\pi$ , nominally  $I = 0$  contributions, both unambiguous and ambiguous — again with the exception of those from the radiative modes  $\pi^0\gamma$  and  $\eta\gamma$ , where the MI contributions have been explicitly determined and the  $I = 0$  contributions determined using the VMD representation contain no MI contamination. The  $3\pi$  MI IB contributions from Tab. I of Ref. [73] are

$$\begin{aligned} [a_\mu^{\text{SD}}]_{3\pi}^{\text{MI}} \times 10^{10} &= -0.13(3), \\ [a_\mu^{\text{int}}]_{3\pi}^{\text{MI}} \times 10^{10} &= -1.03(27), \\ [a_\mu^{\text{LD}}]_{3\pi}^{\text{MI}} \times 10^{10} &= -1.52(40), \\ [a_\mu^{\text{HVP}}]_{3\pi}^{\text{MI}} \times 10^{10} &= -2.68(70). \end{aligned} \quad (17)$$

The corresponding  $I = 0$  non- $3\pi$  totals, obtained by adding to the results of Tab. 2 the  $I = 0$  ambiguous-mode contributions inferable from Tabs. 4 and 3 (again excluding the  $\pi^0\gamma$  and  $\eta\gamma$  mode contributions) are found to be

$$\begin{aligned} [a_\mu^{\text{SD}}]_{\text{non-}3\pi}^{I=0} \times 10^{10} &= 5.04(30), \\ [a_\mu^{\text{int}}]_{\text{non-}3\pi}^{I=0} \times 10^{10} &= 22.53(59), \\ [a_\mu^{\text{LD}}]_{\text{non-}3\pi}^{I=0} \times 10^{10} &= 14.00(14), \\ [a_\mu^{\text{HVP}}]_{\text{non-}3\pi}^{I=0} \times 10^{10} &= 41.56(97). \end{aligned} \quad (18)$$

Adding 1% of these non- $3\pi$ ,  $I = 0$  totals as an additional uncertainty to the results of Eq. (17) and combining these results with the  $I = 1$  MI IB contributions as per Eq. (10), we find the s+lqc MI corrections shown in the 5-th row of Tab. 6.

With the full EM+SIB MI corrections in hand, the remaining IB effects to be dealt with are the EM corrections to the pure  $I = 1$  and  $I = 0$  window contributions. At this point, although several EM contributions have been estimated from experimental data [73–75], other potentially non-negligible EM effects have not (see the discussion in the appendix of Ref. [55]). We have decided, therefore, to rely on lattice EM data for our estimates of the  $I = 1$  and  $I = 0$  EM corrections. As discussed below, these corrections are very small in the lqc case and completely negligible for the s+lqc components, which means that our final results are still (almost) purely data-driven.

We start with a discussion of the lqc EM contributions. For the total HVP, the EM contribution was published in 2021 by BMW [30] and corrected in their more recent paper [33]. The corrected, 2024 result,

$$\Delta_{\text{EM}} a_\mu^{\text{HVP,lqc}} \times 10^{10} = -1.57(42)(35) = -1.57(55), \quad (19)$$

has to be subtracted from our HVP result before comparison with the isospin-symmetric lattice HVP value. BMW also provided the EM correction to the intermediate window

lqc component [30],

$$\Delta_{\text{EM}} a_{\mu}^{\text{int,lqc}} \times 10^{10} = -0.035(59), \quad (20)$$

which constitutes a very small correction with essentially no impact on the final results of our previous works [56, 57].

For the SD and LD windows no number was provided in the BMW papers. This leaves a contribution of about  $1.535 \times 10^{-10}$  to be split between these two windows. Here, we make the assumption that the EM contribution to the lqc component of the SD window is negligible, which means that the entirety of the remaining  $1.535 \times 10^{-10}$  is attributed to the LD window. Two arguments support this assumption. First, a significant portion of the EM contribution to the SD window is amenable to a perturbative calculation. This gives only a tiny correction, which the Mainz collaboration estimated to be  $0.03 \times 10^{-10}$  [47]. Second, the same Mainz paper quotes an initial direct lattice simulation result for the SD EM contribution equal to 0.15(15)% of the sum of the corresponding light and strange connected contributions, corresponding to a central value of  $0.085 \times 10^{-10}$  [47]. This is compatible (though smaller in magnitude) with what we expect to be a conservative estimated bound on the magnitude of the total EM contribution, equal to  $\alpha_{\text{EM}}$  times the total of the unambiguous and ambiguous exclusive-mode SD lqc contributions plus  $\alpha_{\text{EM}}/\pi$  times the corresponding pQCD contribution. This yields the bound

$$\begin{aligned} |\Delta_{\text{EM}} a_{\mu}^{\text{SD,lqc}}| &\leq \alpha_{\text{EM}} \left( [a_{\mu}^{\text{SD,lqc}}]_{\text{unamb}} + [a_{\mu}^{\text{SD,lqc}}]_{\text{amb}} \right) + \frac{\alpha_{\text{EM}}}{\pi} [a_{\mu}^{\text{SD,lqc}}]_{\text{pQCD}} \\ &= \alpha_{\text{EM}} (25.99 + 0.75) \times 10^{-10} + \frac{\alpha_{\text{EM}}}{\pi} 20.28 \times 10^{-10} \\ &= 0.24 \times 10^{-10}, \end{aligned} \quad (21)$$

where  $[a_{\mu}^{\text{SD,lqc}}]_{\text{unamb}}$ ,  $[a_{\mu}^{\text{SD,lqc}}]_{\text{amb}}$ , and  $[a_{\mu}^{\text{SD,lqc}}]_{\text{pQCD}}$  are, respectively, the unambiguous-mode, ambiguous-mode and the pQCD contributions to  $a_{\mu}^{\text{SD,lqc}}$ , given in Tab. 5. This result is a factor of nearly 3 times larger than the uncertainty on the Mainz result. To be conservative, we assign this larger estimate as the uncertainty on our EM SD assumption. Our final estimates for the EM IB contribution to the lqc SD and LD windows are then

$$\begin{aligned} \Delta_{\text{EM}} a_{\mu}^{\text{SD,lqc}} \times 10^{10} &= 0.00(24), \\ \Delta_{\text{EM}} a_{\mu}^{\text{LD,lqc}} \times 10^{10} &= 1.54(55). \end{aligned} \quad (22)$$

For the s+lqd component, the EM corrections to the intermediate window and to the total HVP can be obtained from the published BMW results via the diagrammatic approach explained in detail in Ref. [54]. These corrections turn out to be tiny due, in part, to strong cancellations in the numerically dominant contributions arising from light-quark EM valence-valence connected and disconnected diagrams. For the intermediate window, for example, we obtain the following EM correction to the s+lqd component [56]

$$\Delta_{\text{EM}} a_{\mu}^{\text{int,s+lqd}} \times 10^{10} = 0.012(11), \quad (23)$$

more than 60 times smaller than our final error. Since the final relative uncertainties in the s+lqd SD and LD windows are larger than that of the intermediate window, and

Table 5: KNT19-based [13] results for the lqc component of  $a_\mu^{\text{SD}}$ ,  $a_\mu^{\text{int}}$ ,  $a_\mu^{\text{LD}}$ , and  $a_\mu^{\text{HVP}}$ . The last row gives the final isospin-symmetric results to be compared with lattice-QCD. Uncertainties in the last column take into account the correlations between the three windows. All entries in units of  $10^{-10}$ .

	$a_\mu^{\text{SD,lqc}} \times 10^{10}$	$a_\mu^{\text{int,lqc}} \times 10^{10}$	$a_\mu^{\text{LD,lqc}} \times 10^{10}$	$a_\mu^{\text{HVP,lqc}} \times 10^{10}$
unamb. modes	25.99(21)	186.94(80)	390.6(1.6)	603.6(2.3)
amb. modes	0.75(32)	1.88(61)	0.613(91)	3.2(1.0)
pt. QCD + DVs	20.28(0.10)	11.06(0.16)	0.346(11)	31.68(28)
MI IB correction	-0.07(10)	-0.96(0.30)	-3.19(15)	-4.21(51)
EM IB correction	0.00(24)	0.035(59)	1.54(55)	1.57(55)
Total	46.96(48)	199.0(1.1)	389.9(1.7)	635.8(2.6)

since the EM contributions to s+lqd intermediate window and total HVP results are so small, we believe it to be safe to neglect the EM corrections for the s+lqd component in the case of the SD and LD windows as well.

## 4 Final results

We are now in a position to obtain our final results based on the pre-CMD-3 KNT-19 data compilation. Tabs. 5 and 6 collect all the partial contributions discussed in the previous sections and give, in their last rows, the final results for the isospin-symmetric lqc and s+lqd components of the SD, the intermediate, and the LD windows, as well as of the total HVP. The results for the SD and LD windows are new, while results for the intermediate window and for the total HVP, apart from small updates having very little numerical impact, were already discussed in Refs. [54–57].

In the lqc results of Tab. 5 for the intermediate and LD windows, as well as for the total HVP, the unambiguous-mode contribution overwhelmingly dominates, with an important fraction of the final results arising from the  $2\pi$  channel contribution, which represents 80% for the intermediate window and total HVP results and 88% for the LD window. The lqc components of these windows are, therefore, very sensitive to any issue related to the data-driven contribution from  $e^+e^- \rightarrow \pi^+\pi^-$ . In the SD window, although the contribution from unambiguous modes is still dominant, the pQCD contribution is large (amounting to 43% of the final result), while pQCD gives only a small contributions in all other cases. In Fig. 1 we compare our final results for the lqc component of the three RBC/UKQCD windows to isospin-symmetric lattice-QCD results. In these results, we see that for  $a_\mu^{\text{int,lqc}}$ , as already discussed in Refs. [56, 57], there is a greater-than- $5\sigma$  discrepancy with the most precise lattice results, including the new BMW result [33]. The recently unblinded results from RBC/UKQCD [49] and Mainz [50] for the lqc component of the LD window (in the “BMW world”) also show  $3.5\sigma$  and  $2.5\sigma$  discrepancies, respectively, with respect to our KNT19-based data-driven result. In the SD window, our data-based lqc component, while systematically lower, differs less significantly from the lattice determinations. We recall that the SD window receives an important pQCD contribution, and, since we use perturbation theory, the



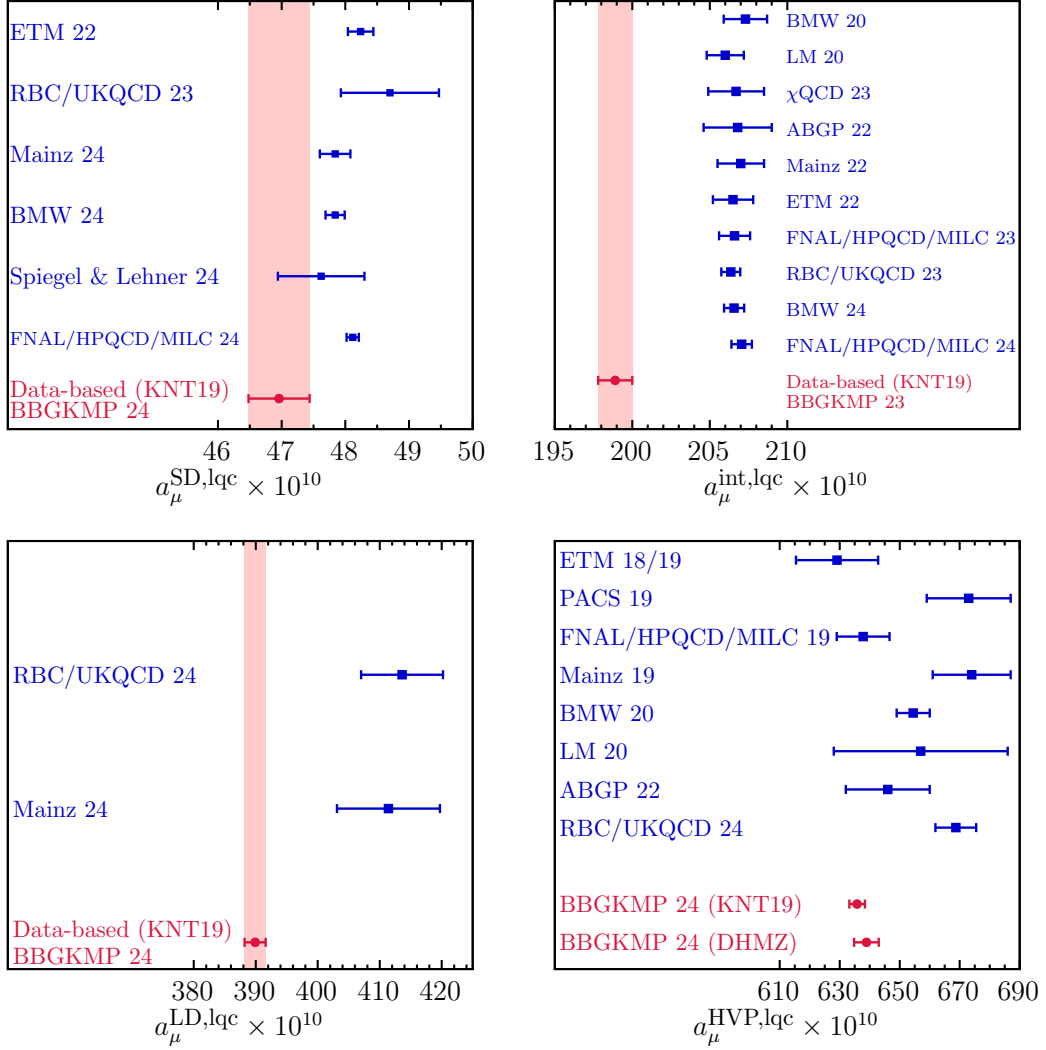


Figure 1: Data-driven KNT19-based [13] results for the lqc components of the RBC/UKQCD windows compared with isospin-symmetric lattice-QCD determinations of the same quantities. (Upper-left panel) Data-driven  $a_\mu^{\text{SD},\text{lqc}}$  compared with results from Refs. [33, 43, 45–48]. Results from this work are labeled “BBGKMP 24.” (Upper-right panel) Data-driven  $a_\mu^{\text{int},\text{lqc}}$  compared with results from Refs. [30, 39–46]. (Bottom-left panel) Data-driven  $a_\mu^{\text{LD},\text{lqc}}$  compared with the recent results of Refs. [49, 50]. (Bottom-right panel) Data-driven  $a_\mu^{\text{HVP},\text{lqc}}$  compared with results from Refs. [30, 39, 41, 49, 51, 76–79].

final result in this case is less dominated by exclusive-mode experimental data. Given the reduced role of  $\rho$ -region  $2\pi$  exclusive-mode contributions for the SD window, the reduced difference between the data-driven and lattice results in the SD case is also compatible with the hypothesis that all of the observed discrepancies between data-driven and lattice results have their source in contributions from the  $\rho$  peak region.

We turn now to the results for the s+lqd components, given in Tab. 6. There are three

Table 6: KNT19-based [13] results for the s+lq component of  $a_\mu^{\text{SD}}$ ,  $a_\mu^{\text{int}}$ ,  $a_\mu^{\text{LD}}$ , and  $a_\mu^{\text{HVP}}$ . The last row gives the final isospin-symmetric results to be compared with lattice-QCD. Uncertainties in the last column take into account the correlations between the three windows. All entries in units of  $10^{-10}$ .

	$a_\mu^{\text{SD,s+lq}} \times 10^{10}$	$a_\mu^{\text{int,s+lq}} \times 10^{10}$	$a_\mu^{\text{LD,s+lq}} \times 10^{10}$	$a_\mu^{\text{HVP,s+lq}} \times 10^{10}$
unamb. total	0.903(68)	1.99(38)	-13.32(57)	-10.43(98)
amb. total	4.25(33)	21.86(64)	15.96(18)	42.1(1.1)
pt. QCD + DVs	3.93(11)	2.00(17)	0.054(13)	5.99(30)
MI IB correction	0.137(60)	1.13(35)	1.84(42)	3.10(82)
Total	9.21(36)	26.98(84)	4.53(73)	40.7(1.7)

recent lattice determinations of the relevant components of the SD window [33, 46, 47], all in good agreement. BMW [33] finds, for the strange-quark-connected and light-quark-disconnected contributions, the results,  $9.04(7) \times 10^{-10}$  and  $-0.0007(102) \times 10^{-10}$ , respectively. The corresponding correlation is not quoted, so we know only that the uncertainty on the BMW s+lq sum must lie in the range  $(0.07 \pm 0.01) \times 10^{-10}$ . The Mainz collaboration [47] finds a compatible result,  $9.072(59) \times 10^{-10}$ , for the strange-quark connected contribution, and comments that the strange-quark- and light-quark-disconnected contributions were found to be irrelevant at the level of precision of the strange connected result. Finally, FNAL/HPQCD/MILC quotes results  $9.103(3)(21) \times 10^{-10}$  and  $-0.0002(6)(53) \times 10^{-10}$  for the strange-quark-connected and light-quark-disconnected contributions, with a 0.13 correlation coefficient between them [46].

Taking the most conservative assessment of the BMW error, and following Mainz in neglecting their disconnected contribution, we find for the lattice versions of the s+lq component of the SD window, the results

$$\begin{aligned}
a_\mu^{\text{SD,s+lq}} \times 10^{10} &= 9.04(8) && \text{(BMW 24 [33])}, \\
a_\mu^{\text{SD,s+lq}} \times 10^{10} &= 9.072(59) && \text{(Mainz 24 [47])}, \\
a_\mu^{\text{SD,s+lq}} \times 10^{10} &= 9.103(22) && \text{(FNAL/HPQCD/MILC 24 [46])}.
\end{aligned} \tag{24}$$

These are all in excellent agreement with our data-driven determination,  $a_\mu^{\text{SD,s+lq}} \times 10^{-10} = 9.21(36)$ , though in this case the data-driven uncertainty is significantly larger than that on the lattice results. A visual account of this comparison is given in the left-hand panel of Fig. 2. For the s+lq contribution to the LD window, we obtain  $4.53(73) \times 10^{-10}$ . The only lattice determination of this quantity, by the Mainz collaboration, gives

$$a_\mu^{\text{LD,s+lq}} \times 10^{10} = 1.3(2.4) \quad \text{(Mainz 24 [50, 80])}, \tag{25}$$

which is compatible, within  $1.3\sigma$ , with our data-driven result. The results for  $a_\mu^{\text{int,s+lq}}$  and  $a_\mu^{\text{HVP,s+lq}}$ , in turn, agree well with the lattice determinations of Refs. [30, 34, 52, 53] and Refs. [30, 34, 42, 43], respectively, as discussed in our previous works [54, 57]. The right-hand panel of Fig. 2 shows an updated visual account of this comparison for  $a_\mu^{\text{int,s+lq}}$  including the new result of Ref. [46], also in very good agreement with our data-driven determination.

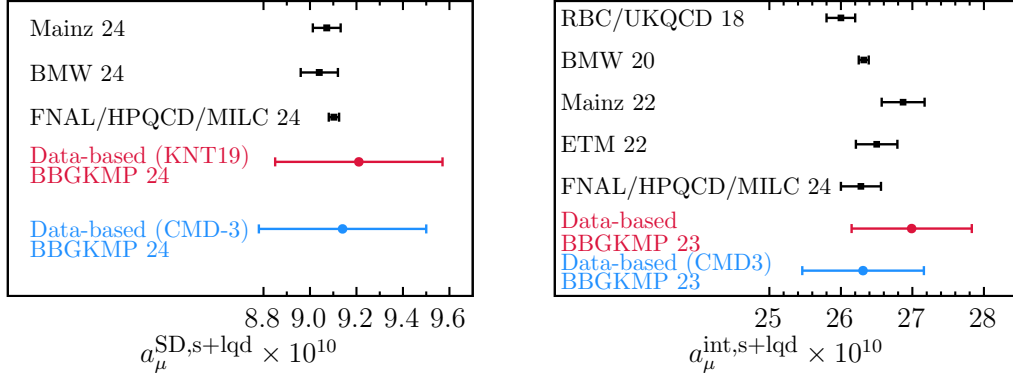


Figure 2: Data-driven results for the s+lq components of the RBC/UKQCD SD and intermediate windows compared with isospin-symmetric lattice determinations of the same quantities. (Left-hand panel) Data-driven results for  $a_\mu^{\text{SD},s+lq}$  compared with results from Refs. [33, 46, 47]. See the text for a discussion of how the lattice numbers were obtained. (Right-hand panel) Data-driven results for  $a_\mu^{\text{int},s+lq}$  compared with results from Refs. [30, 34, 42, 43, 46]. Results from this work are labeled “BBGKMP 24.”

We close this section with a short discussion of the correlations between the results for the different windows. Clearly, results for the same component (lqc or s+lq) of the different windows are expected to be highly correlated, since they are simply differently weighted integrals of the same (lqc or s+lq) spectral data. Although the central values of the final window results in Tabs. 5 and 6 can be directly summed to reproduce the  $a_\mu^{\text{HVP}}$  values in the last column, combining the errors on the three window quantities to obtain that on  $a_\mu^{\text{HVP}}$  requires knowledge of the correlations between the window errors.

The correlation between a pair of such window results is straightforwardly obtained from the errors on the two individual windows (given in Tabs. 5 and 6 above) in combination with a separate, direct evaluation of the error on the sum of the two windows. As input to this assessment, we have assumed that the MI IB contributions obtained from Ref. [73] are 100% correlated, which is both conservative and supported by the uncertainties given in the original reference. The results, however, do not include effects due to the  $I = 1$  and  $I = 0$  EM IB corrections, which do, however, enter the computation of the lqc components. EM contributions to the errors on the sums of window pairs, which would be needed to incorporate these effects, cannot be reliably included because the information available from Refs. [30, 33], though including the central values and errors for the intermediate window and total HVP, does not include the corresponding correlation. We do not, however, expect this limitation to be numerically relevant since the contribution of the EM IB corrections to the final central values and uncertainties are small.

With the strategy described above, we obtain the following non-trivial correlation coefficients for the lqc components of the three RBC/UKQCD windows

$$\begin{aligned}\rho_{\text{SD,int}} &= 0.894, \\ \rho_{\text{int,LD}} &= 0.509, \\ \rho_{\text{SD,LD}} &= 0.341.\end{aligned}\tag{26}$$

Table 7: Exploratory results for the lqc component of  $a_\mu^{\text{SD}}$ ,  $a_\mu^{\text{int}}$ ,  $a_\mu^{\text{LD}}$ , and  $a_\mu^{\text{HVP}}$  using the CMD-3  $\pi^+\pi^-$  data [32] in the energy region covered by the CMD-3 experiment and KNT19 data [13] otherwise. Uncertainties in the last column take into account the correlations between the three windows. All entries in units of  $10^{-10}$ .

	$a_\mu^{\text{SD,lqc}} \times 10^{10}$	$a_\mu^{\text{int,lqc}} \times 10^{10}$	$a_\mu^{\text{LD,lqc}} \times 10^{10}$	$a_\mu^{\text{HVP,lqc}} \times 10^{10}$
unambiguous total	26.67(25)	193.8(1.5)	407.2(3.2)	627.7(4.8)
ambiguous total	0.75(32)	1.88(61)	0.613(91)	3.2(1.0)
pt. QCD + DVs	20.28(0.10)	11.06(0.16)	0.346(11)	31.68(28)
MI IB correction	-0.07(10)	-0.96(0.30)	-3.19(15)	-4.21(51)
EM IB correction	0.00(24)	0.035(59)	1.54(55)	1.57(55)
Total	47.63(50)	205.8(1.6)	406.5(3.2)	660.0(4.9)

The results for the correlations of the s+lqd components are

$$\begin{aligned}
\rho_{\text{SD,int}}^{\text{s+lqd}} &= 0.888, \\
\rho_{\text{int,LD}}^{\text{s+lqd}} &= 0.687, \\
\rho_{\text{SD,LD}}^{\text{s+lqd}} &= 0.228.
\end{aligned} \tag{27}$$

With these correlation coefficients and standard error propagation, one can verify that the addition of the three window results does reproduce the HVP totals shown in the fifth columns of Tabs. 5 and 6.

## 5 Potential impact of CMD-3 results

Table 8: Exploratory results for the s+lqd component of  $a_\mu^{\text{SD}}$ ,  $a_\mu^{\text{int}}$ ,  $a_\mu^{\text{LD}}$ , and  $a_\mu^{\text{HVP}}$  using the CMD-3  $\pi^+\pi^-$  data [32] in the energy region covered by the CMD-3 experiment and KNT19 data [13] otherwise. Uncertainties in the last column take into account the correlations between the three windows. All entries in units of  $10^{-10}$ .

	$a_\mu^{\text{SD,s+lqd}} \times 10^{10}$	$a_\mu^{\text{int,s+lqd}} \times 10^{10}$	$a_\mu^{\text{LD,s+lqd}} \times 10^{10}$	$a_\mu^{\text{HVP,s+lqd}} \times 10^{10}$
unamb. total	0.836(69)	1.31(40)	-14.89(63)	-12.7(1.1)
amb. total	4.25(33)	21.86(64)	15.96(18)	42.1(1.1)
pt. QCD + DVs	3.93(11)	2.00(17)	0.054(13)	5.99(30)
MI IB correction	0.137(60)	1.13(35)	1.84(42)	3.10(82)
Total	9.14(36)	26.30(85)	2.96(79)	38.4(1.7)

In this section we investigate the potential impact of the new CMD-3  $e^+e^- \rightarrow \pi^+\pi^-$  cross-sections [32] on the results discussed in the previous section. The CMD-3 cross sections, as is now well known, are significantly higher than those of earlier experiments in the region around the  $\rho$  peak, which gives a very prominent contribution to  $a_\mu^{\text{HVP}}$ . The

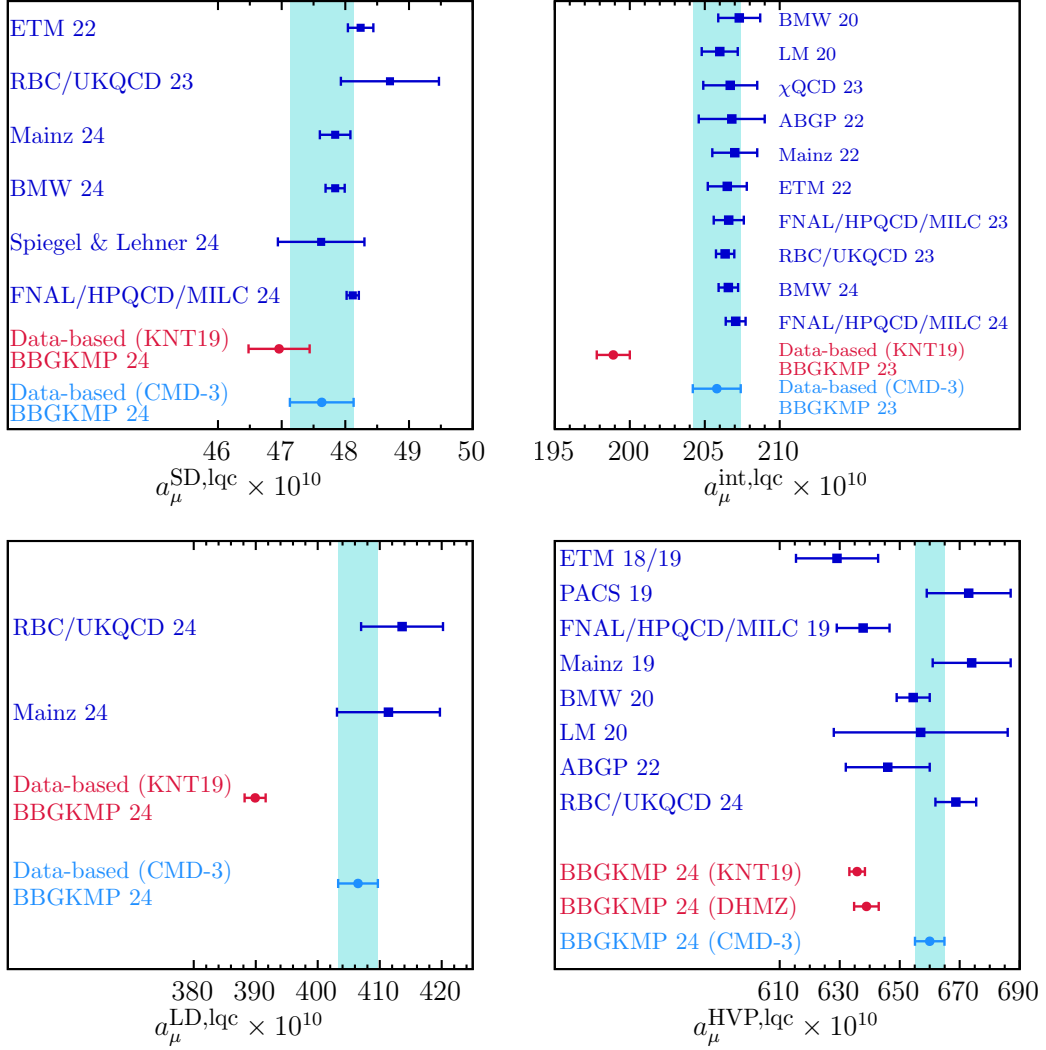


Figure 3: Exploratory data-driven results for the lqc components of the RBC/UKQCD windows employing CMD-3  $2\pi$  data [32] in the energy region covered by the CMD-3 experiment and KNT19 data [13] elsewhere (light blue) in comparison with data-driven results obtained employing KNT19 data only (red), and isospin-symmetric lattice-QCD determinations of the same quantities. Results from this work are labeled “BBGKMP 24.” (Upper-left panel) Data-driven results for  $a_\mu^{\text{SD},\text{lqc}}$  compared with results from Refs. [33, 43, 45–48]. (Upper-right panel) Data-driven results for  $a_\mu^{\text{int},\text{lqc}}$  compared with results from Refs. [30, 39–46]. (Bottom-left panel) Data-driven results for  $a_\mu^{\text{LD},\text{lqc}}$  compared with the recent results of Refs. [49, 50]. (Bottom-right panel) Data-driven  $a_\mu^{\text{HVP},\text{lqc}}$  compared with results from Refs. [30, 39, 41, 49, 51, 76–79].

shift in the  $2\pi$  contribution produced by the CMD-3 data would, in fact, be sufficient to eliminate the discrepancy between the experimental result for  $a_\mu$  and the White Paper SM expectation obtained using the pre-CMD-3 dispersive HVP result. Unfortunately, the disagreement between the  $e^+e^- \rightarrow \pi^+\pi^-$  cross sections obtained by CMD-3 and

earlier experiments is sufficiently large that a meaningful combination of all  $2\pi$ -channel data appears impossible, at present. Given this state of affairs, we perform, in this section, a preliminary exploration, in the spirit of our previous work [57], in which KNT19  $2\pi$   $R(s)$  data is simply replaced by CMD-3 results in the region covered by the CMD-3 experiment, *i.e.*, for center-of-mass energies in the range 0.327 GeV to 1.199 GeV. For this exercise, we apply vacuum polarization (VP) corrections to the physical cross sections obtained from the CMD-3 pion form factor results and dress the resulting bare cross sections with final state radiation (FSR) correction factors, using the same VP and FSR corrections factors employed by CMD-3.<sup>8</sup>

The results of this exploration for the KNT19 exclusive-mode-region  $\pi^+\pi^-$  contributions to the RBC/UKQCD windows and  $a_\mu^{\text{HVP}}$ ,

$$\begin{aligned} [a_\mu^{\text{SD}}]_{2\pi}^{I=1} \times 10^{10} &= 15.53(13), \\ [a_\mu^{\text{int}}]_{2\pi}^{I=1} \times 10^{10} &= 150.3(1.2), \\ [a_\mu^{\text{LD}}]_{2\pi}^{I=1} \times 10^{10} &= 359.4(2.8), \\ [a_\mu^{\text{HVP}}]_{2\pi}^{I=1} \times 10^{10} &= 525.2(4.2) \end{aligned} \tag{28}$$

are all significantly larger than the purely-KNT19-based counterparts given in the third row of Tab. 1. The shift for  $a_\mu^{\text{HVP}}$ , for example, is about  $+21.5 \times 10^{-10}$ . These exploratory CMD-3-based  $2\pi$  results can be combined with the KNT19-based contributions from all other exclusive modes and the resulting modified exclusive-mode sums used to reevaluate the lqc and s+lqd components of the three windows. The results of this exercise are given in Tab. 7 and 8.

As can be seen in the last row of Tab. 7, the use of the CMD-3  $2\pi$  data produces larger lqc contributions for all RBC/UKQCD windows. These larger results, moreover, all agree very well with lattice-QCD determinations of the same quantities, as shown in Fig. 3. The CMD-3-based result for  $a_\mu^{\text{HVP}}$  would also produce the shift required to make the data-driven determination of the full  $a_\mu$  compatible with experiment. A recent analysis [81] provides further evidence for the agreement between the lattice results and the KNT19 data modified with the results for the two-pion mode from CMD-3.

In the CMD-3-based s+lqd results of Tab. 8, we see that the shifts for the SD and intermediate windows are very small and thus do not spoil the very good agreement observed above between the lattice determinations of these quantities and the KNT19-based results of Tab. 6, see Fig. 2. For the LD s+lqd component, where a strong cancellation between the unambiguous- and ambiguous-mode totals is observed, the shift is somewhat larger and the CMD-3-based result is  $2.96(79) \times 10^{-10}$ . This shift reduces the difference between the only lattice determination of this quantity, given in Eq. (25), and the data-driven result from  $1.3\sigma$  to  $0.7\sigma$ . Finally, the result for  $a_\mu^{\text{HVP}, \text{s+lqd}}$ , which is shifted from  $40.7(1.7) \times 10^{-10}$  to  $38.4(1.7) \times 10^{-10}$ , remains compatible with lattice-QCD determinations.

## 6 Conclusions

In this paper, we concluded the data-driven evaluation of the lqc and s+lqd components of the three RBC/UKQCD windows for  $a_\mu^{\text{HVP}}$  providing, for the first time, results

<sup>8</sup>We thank Fedor Ignatov for providing the VP corrections used by CMD-3.

for the SD and LD windows. The method we employed is the same as that used in our previous determinations of the lqc and s+lqd components of the total  $a_\mu^{\text{HVP}}$  [54, 55] and RBC/UKQCD intermediate window [56], as well as those of the alternate intermediate window of Ref. [41] and other windows proposed in the literature [57, 82]. We have shown, in this series of papers, that the data-driven computation can be reorganized to make possible the extraction of isospin-symmetric results for these key components of  $a_\mu^{\text{HVP}}$ , and hence also detailed, precision comparisons with results obtained from the lattice.

Our data-driven results for the s+lqd components, obtained using the (pre-CMD-3) KNT19 data compilation, agree well with lattice determinations, with no significant discrepancies within our uncertainties. In contrast, results for the data-driven lqc components of the intermediate and LD windows obtained from the KNT19 data compilation, summarized in Tab. 5 and Fig. 1, show a strong tension with lattice results. In the case of the intermediate window, there is a greater-than- $5\sigma$  incompatibility between our data-driven determination and the most precise lattice numbers, while for the LD window a significant discrepancy is found with respect to the the two recently released, unblinded lattice results. Results for the SD window are also systematically lower than the lattice determinations, though, with our larger data-driven uncertainty, the resulting data-driven versus lattice differences are of lower significance than those of the LD and intermediate window cases.

It is important to note that the data-driven results for the lqc components of the intermediate and LD windows are dominated by the  $\pi^+\pi^-$  contributions, which represent 80% and 88% of the totals, respectively. These results are, therefore, sensitive to the discrepancies in the different measurements of the  $e^+e^- \rightarrow \pi^+\pi^-$  cross sections. The results for the SD window, in contrast, are less strongly sensitive to the  $\pi^+\pi^-$  contribution and receive an important contribution from pQCD.

These observations raise the question of the potential impact of the CMD-3  $2\pi$  data, which we investigated, in an exploratory framework, in Sec. 5. In this preliminary analysis, we simply replaced the KNT19  $2\pi$  data with CMD-3 results in the region covered by the CMD-3 experiment. The results for the lqc component obtained using CMD-3 data, summarized in Tab. 7 and Fig. 3, are in very good agreement with the lattice determinations. The CMD-3-induced shifts in the s+lqd components are, of course, a factor of 10 smaller than those in the lqc components, and it is thus not surprising that, as was the case for s+lqd results based on pre-CMD-3 data, the CMD-3-modified s+lqd results, given in Tab. 8, remain compatible with the lattice. In the single case where a larger shift is observed, namely for the s+lqd LD window component, the CMD-3-based result brings the central value into even closer agreement with that of the recent lattice result from Mainz, Eq. (25). This demonstrates explicitly that shifts in the  $\rho$ -peak-region  $2\pi$  cross sections, such as those observed in the CMD-3 data, can produce data-driven lqc components compatible with the lattice, without disturbing the good agreement observed for the SD, the intermediate window, and the total HVP s+lqd components.

We emphasize that our comparisons between data-driven and lattice results are based on employing the KNT19 (and CMD-3) data for the data-driven RBC/UKQCD window results. At present, with the exclusive-mode distributions and covariances of the DHMZ collaboration [10, 12] not publicly available, it is not possible to carry out these same comparisons using DHMZ input. This is in contrast to the situation for  $a_\mu^{\text{HVP}}$ , where



DHMZ integrated exclusive-mode-contribution results are publicly available [12], and these allowed us to obtain, in Refs. [54, 55], DHMZ-exclusive-mode-based data-driven determinations of the lqc and s+lqd components of  $a_\mu^{\text{HVP}}$ . With the recent 2024 BMW correction to their previous  $a_\mu^{\text{HVP}}$  EM IB contribution result, our previous data-driven lqc result [55] is now shifted slightly, to

$$a_\mu^{\text{HVP,lqc}} \times 10^{10} = 638.9(4.1) \quad (\text{DHMZ based [12]}). \quad (29)$$

## Acknowledgements

We thank Aida El-Khadra, Simon Kuberski, and Hartmut Wittig for providing results from as yet unpublished lattice QCD analyses. DB's work was supported by the São Paulo Research Foundation (FAPESP) grant No. 2021/06756-6 and by CNPq grant No. 308979/2021-4. MG is supported by the U.S. Department of Energy, Office of Science, Office of High Energy Physics, under Award No. DE-SC0013682. AK is supported by The Royal Society (URF\R1\231503). KM is supported by a grant from the Natural Sciences and Engineering Research Council of Canada. SP is supported by the Spanish Ministerio de Ciencia e Innovacion, grants PID2020-112965GB-I00 and PID2023-146142NB-I00, and by the Departament de Recerca i Universitats from Generalitat de Catalunya to the Grup de Recerca 00649 (Codi: 2021 SGR 00649). IFAE is partially funded by the CERCA program of the Generalitat de Catalunya.

## References

- [1] MUON  $g-2$  collaboration, B. Abi et al., *Measurement of the positive muon anomalous magnetic moment to 0.46 ppm*, *Phys. Rev. Lett.* **126** (2021) 141801 [2104.03281].
- [2] MUON  $g-2$  collaboration, T. Albahri et al., *Measurement of the anomalous precession frequency of the muon in the Fermilab Muon  $g-2$  Experiment*, *Phys. Rev. D* **103** (2021) 072002 [2104.03247].
- [3] MUON  $G-2$  collaboration, D. P. Aguillard et al., *Measurement of the Positive Muon Anomalous Magnetic Moment to 0.20 ppm*, *Phys. Rev. Lett.* **131** (2023) 161802 [2308.06230].
- [4] MUON  $g-2$  collaboration, G. W. Bennett et al., *Final report of the muon E821 anomalous magnetic moment measurement at BNL*, *Phys. Rev. D* **73** (2006) 072003 [hep-ex/0602035].
- [5] T. Aoyama et al., *The anomalous magnetic moment of the muon in the Standard Model*, *Phys. Rept.* **887** (2020) 1 [2006.04822].
- [6] T. Aoyama, M. Hayakawa, T. Kinoshita and M. Nio, *Complete Tenth-Order QED Contribution to the Muon  $g-2$* , *Phys. Rev. Lett.* **109** (2012) 111808 [1205.5370].
- [7] T. Aoyama, T. Kinoshita and M. Nio, *Theory of the Anomalous Magnetic Moment of the Electron*, *Atoms* **7** (2019) 28.

- [8] A. Czarnecki, W. J. Marciano and A. Vainshtein, *Refinements in electroweak contributions to the muon anomalous magnetic moment*, *Phys. Rev. D* **67** (2003) 073006 [[hep-ph/0212229](#)].
- [9] C. Gnendiger, D. Stöckinger and H. Stöckinger-Kim, *The electroweak contributions to  $(g - 2)_\mu$  after the Higgs boson mass measurement*, *Phys. Rev. D* **88** (2013) 053005 [[1306.5546](#)].
- [10] M. Davier, A. Hoecker, B. Malaescu and Z. Zhang, *Reevaluation of the hadronic vacuum polarisation contributions to the Standard Model predictions of the muon  $g - 2$  and  $\alpha(m_Z^2)$  using newest hadronic cross-section data*, *Eur. Phys. J. C* **77** (2017) 827 [[1706.09436](#)].
- [11] A. Keshavarzi, D. Nomura and T. Teubner, *Muon  $g - 2$  and  $\alpha(M_Z^2)$ : a new data-based analysis*, *Phys. Rev. D* **97** (2018) 114025 [[1802.02995](#)].
- [12] M. Davier, A. Hoecker, B. Malaescu and Z. Zhang, *A new evaluation of the hadronic vacuum polarisation contributions to the muon anomalous magnetic moment and to  $\alpha(m_Z^2)$* , *Eur. Phys. J. C* **80** (2020) 241 [[1908.00921](#)].
- [13] A. Keshavarzi, D. Nomura and T. Teubner,  *$g - 2$  of charged leptons,  $\alpha(M_Z^2)$ , and the hyperfine splitting of muonium*, *Phys. Rev. D* **101** (2020) 014029 [[1911.00367](#)].
- [14] G. Colangelo, M. Hoferichter and P. Stoffer, *Two-pion contribution to hadronic vacuum polarization*, *JHEP* **02** (2019) 006 [[1810.00007](#)].
- [15] M. Hoferichter, B.-L. Hoid and B. Kubis, *Three-pion contribution to hadronic vacuum polarization*, *JHEP* **08** (2019) 137 [[1907.01556](#)].
- [16] B.-L. Hoid, M. Hoferichter and B. Kubis, *Hadronic vacuum polarization and vector-meson resonance parameters from  $e^+e^- \rightarrow \pi^0\gamma$* , *Eur. Phys. J. C* **80** (2020) 988 [[2007.12696](#)].
- [17] A. Kurz, T. Liu, P. Marquard and M. Steinhauser, *Hadronic contribution to the muon anomalous magnetic moment to next-to-next-to-leading order*, *Phys. Lett. B* **734** (2014) 144 [[1403.6400](#)].
- [18] K. Melnikov and A. Vainshtein, *Hadronic light-by-light scattering contribution to the muon anomalous magnetic moment revisited*, *Phys. Rev. D* **70** (2004) 113006 [[hep-ph/0312226](#)].
- [19] P. Masjuan and P. Sanchez-Puertas, *Pseudoscalar-pole contribution to the  $(g_\mu - 2)$ : a rational approach*, *Phys. Rev. D* **95** (2017) 054026 [[1701.05829](#)].
- [20] G. Colangelo, M. Hoferichter, M. Procura and P. Stoffer, *Rescattering effects in the hadronic-light-by-light contribution to the anomalous magnetic moment of the muon*, *Phys. Rev. Lett.* **118** (2017) 232001 [[1701.06554](#)].
- [21] G. Colangelo, M. Hoferichter, M. Procura and P. Stoffer, *Dispersion relation for hadronic light-by-light scattering: two-pion contributions*, *JHEP* **04** (2017) 161 [[1702.07347](#)].

- [22] M. Hoferichter, B.-L. Hoid, B. Kubis, S. Leupold and S. P. Schneider, *Pion-pole contribution to hadronic light-by-light scattering in the anomalous magnetic moment of the muon*, *Phys. Rev. Lett.* **121** (2018) 112002 [[1805.01471](#)].
- [23] M. Hoferichter, B.-L. Hoid, B. Kubis, S. Leupold and S. P. Schneider, *Dispersion relation for hadronic light-by-light scattering: pion pole*, *JHEP* **10** (2018) 141 [[1808.04823](#)].
- [24] A. Gérardin, H. B. Meyer and A. Nyffeler, *Lattice calculation of the pion transition form factor with  $N_f = 2 + 1$  Wilson quarks*, *Phys. Rev. D* **100** (2019) 034520 [[1903.09471](#)].
- [25] J. Bijnens, N. Hermansson-Truedsson and A. Rodríguez-Sánchez, *Short-distance constraints for the HLbL contribution to the muon anomalous magnetic moment*, *Phys. Lett. B* **798** (2019) 134994 [[1908.03331](#)].
- [26] G. Colangelo, F. Hagelstein, M. Hoferichter, L. Laub and P. Stoffer, *Short-distance constraints on hadronic light-by-light scattering in the anomalous magnetic moment of the muon*, *Phys. Rev. D* **101** (2020) 051501 [[1910.11881](#)].
- [27] G. Colangelo, F. Hagelstein, M. Hoferichter, L. Laub and P. Stoffer, *Longitudinal short-distance constraints for the hadronic light-by-light contribution to  $(g - 2)_\mu$  with large- $N_c$  Regge models*, *JHEP* **03** (2020) 101 [[1910.13432](#)].
- [28] G. Colangelo, M. Hoferichter, A. Nyffeler, M. Passera and P. Stoffer, *Remarks on higher-order hadronic corrections to the muon  $g - 2$* , *Phys. Lett. B* **735** (2014) 90 [[1403.7512](#)].
- [29] T. Blum, N. Christ, M. Hayakawa, T. Izubuchi, L. Jin, C. Jung et al., *Hadronic Light-by-Light Scattering Contribution to the Muon Anomalous Magnetic Moment from Lattice QCD*, *Phys. Rev. Lett.* **124** (2020) 132002 [[1911.08123](#)].
- [30] S. Borsanyi et al., *Leading hadronic contribution to the muon magnetic moment from lattice QCD*, *Nature* **593** (2021) 51 [[2002.12347](#)].
- [31] C. Aubin, T. Blum, C. Tu, M. Golterman, C. Jung and S. Peris, *Light quark vacuum polarization at the physical point and contribution to the muon  $g - 2$* , *Phys. Rev. D* **101** (2020) 014503 [[1905.09307](#)].
- [32] CMD-3 collaboration, F. V. Ignatov et al., *Measurement of the  $e^+e^- \rightarrow \pi^+\pi^-$  cross section from threshold to 1.2 GeV with the CMD-3 detector*, *Phys. Rev. D* **109** (2024) 112002 [[2302.08834](#)].
- [33] A. Boccaletti et al., *High precision calculation of the hadronic vacuum polarisation contribution to the muon anomaly*, [2407.10913](#).
- [34] RBC, UKQCD collaboration, T. Blum, P. A. Boyle, V. Gülpers, T. Izubuchi, L. Jin, C. Jung et al., *Calculation of the hadronic vacuum polarization contribution to the muon anomalous magnetic moment*, *Phys. Rev. Lett.* **121** (2018) 022003 [[1801.07224](#)].

- [35] G. Colangelo, A. X. El-Khadra, M. Hoferichter, A. Keshavarzi, C. Lehner, P. Stoffer et al., *Data-driven evaluations of Euclidean windows to scrutinize hadronic vacuum polarization*, *Phys. Lett. B* **833** (2022) 137313 [[2205.12963](#)].
- [36] H. Wittig, *Progress on  $(g - 2)_\mu$  from Lattice QCD*, in *57th Rencontres de Moriond on Electroweak Interactions and Unified Theories*, 6, 2023, [2306.04165](#).
- [37] J. A. Miranda and P. Roig, *New  $\tau$ -based evaluation of the hadronic contribution to the vacuum polarization piece of the muon anomalous magnetic moment*, *Phys. Rev. D* **102** (2020) 114017 [[2007.11019](#)].
- [38] P. Masjuan, A. Miranda and P. Roig,  *$\tau$  data-driven evaluation of Euclidean windows for the hadronic vacuum polarization*, [2305.20005](#).
- [39] C. Lehner and A. S. Meyer, *Consistency of hadronic vacuum polarization between lattice QCD and the R-ratio*, *Phys. Rev. D* **101** (2020) 074515 [[2003.04177](#)].
- [40] CHIQCD collaboration, G. Wang, T. Draper, K.-F. Liu and Y.-B. Yang, *Muon  $g-2$  with overlap valence fermions*, *Phys. Rev. D* **107** (2023) 034513 [[2204.01280](#)].
- [41] C. Aubin, T. Blum, M. Golterman and S. Peris, *Muon anomalous magnetic moment with staggered fermions: Is the lattice spacing small enough?*, *Phys. Rev. D* **106** (2022) 054503 [[2204.12256](#)].
- [42] M. Cè et al., *Window observable for the hadronic vacuum polarization contribution to the muon  $g-2$  from lattice QCD*, *Phys. Rev. D* **106** (2022) 114502 [[2206.06582](#)].
- [43] EXTENDED TWISTED MASS collaboration, C. Alexandrou et al., *Lattice calculation of the short and intermediate time-distance hadronic vacuum polarization contributions to the muon magnetic moment using twisted-mass fermions*, *Phys. Rev. D* **107** (2023) 074506 [[2206.15084](#)].
- [44] FERMILAB LATTICE, HPQCD, MILC collaboration, A. Bazavov et al., *Light-quark connected intermediate-window contributions to the muon  $g-2$  hadronic vacuum polarization from lattice QCD*, *Phys. Rev. D* **107** (2023) 114514 [[2301.08274](#)].
- [45] RBC, UKQCD collaboration, T. Blum et al., *Update of Euclidean windows of the hadronic vacuum polarization*, *Phys. Rev. D* **108** (2023) 054507 [[2301.08696](#)].
- [46] FERMILAB LATTICE, LATTICE-HPQCD, MILC collaboration, A. Bazavov et al., *Hadronic vacuum polarization for the muon  $g - 2$  from lattice QCD: Complete short and intermediate windows*, [2411.09656](#).
- [47] S. Kuberski, M. Cè, G. von Hippel, H. B. Meyer, K. Ottnad, A. Risch et al., *Hadronic vacuum polarization in the muon  $g - 2$ : the short-distance contribution from lattice QCD*, *JHEP* **03** (2024) 172 [[2401.11895](#)].
- [48] S. Spiegel and C. Lehner, *A high-precision continuum limit study of the HVP short-distance window*, [2410.17053](#).
- [49] RBC, UKQCD collaboration, T. Blum et al., *The long-distance window of the hadronic vacuum polarization for the muon  $g - 2$* , [2410.20590](#).

- [50] D. Djukanovic, G. von Hippel, S. Kuberski, H. B. Meyer, N. Miller, K. Ottnad et al., *The hadronic vacuum polarization contribution to the muon  $g - 2$  at long distances*, [2411.07969](#).
- [51] A. Gérardin, M. Cè, G. von Hippel, B. Hörz, H. B. Meyer, D. Mohler et al., *The leading hadronic contribution to  $(g - 2)_\mu$  from lattice QCD with  $N_f = 2 + 1$  flavours of  $O(a)$  improved Wilson quarks*, *Phys. Rev. D* **100** (2019) 014510 [[1904.03120](#)].
- [52] BUDAPEST-MARSEILLE-WUPPERTAL collaboration, S. Borsanyi et al., *Hadronic vacuum polarization contribution to the anomalous magnetic moments of leptons from first principles*, *Phys. Rev. Lett.* **121** (2018) 022002 [[1711.04980](#)].
- [53] T. Blum, P. A. Boyle, T. Izubuchi, L. Jin, A. Jüttner, C. Lehner et al., *Calculation of the hadronic vacuum polarization disconnected contribution to the muon anomalous magnetic moment*, *Phys. Rev. Lett.* **116** (2016) 232002 [[1512.09054](#)].
- [54] D. Boito, M. Golterman, K. Maltman and S. Peris, *Evaluation of the three-flavor quark-disconnected contribution to the muon anomalous magnetic moment from experimental data*, *Phys. Rev. D* **105** (2022) 093003 [[2203.05070](#)].
- [55] D. Boito, M. Golterman, K. Maltman and S. Peris, *Data-based determination of the isospin-limit light-quark-connected contribution to the anomalous magnetic moment of the muon*, *Phys. Rev. D* **107** (2023) 074001 [[2211.11055](#)].
- [56] G. Benton, D. Boito, M. Golterman, A. Keshavarzi, K. Maltman and S. Peris, *Data-Driven Determination of the Light-Quark Connected Component of the Intermediate-Window Contribution to the Muon  $g - 2$* , *Phys. Rev. Lett.* **131** (2023) 251803 [[2306.16808](#)].
- [57] G. Benton, D. Boito, M. Golterman, A. Keshavarzi, K. Maltman and S. Peris, *Data-driven estimates for light-quark-connected and strange-plus-disconnected hadronic  $g - 2$  window quantities*, *Phys. Rev. D* **109** (2024) 036010 [[2311.09523](#)].
- [58] S. J. Brodsky and E. De Rafael, *Suggested Boson-Lepton Pair Couplings and the Anomalous Magnetic Moment of the Muon*, *Phys. Rev.* **168** (1968) 1620.
- [59] B. E. Lautrup and E. De Rafael, *Calculation of the sixth-order contribution from the fourth-order vacuum polarization to the difference of the anomalous magnetic moments of muon and electron*, *Phys. Rev.* **174** (1968) 1835.
- [60] M. Gourdin and E. De Rafael, *Hadronic contributions to the muon  $g$ -factor*, *Nucl. Phys. B* **10** (1969) 667.
- [61] D. Bernecker and H. B. Meyer, *Vector Correlators in Lattice QCD: Methods and applications*, *Eur. Phys. J. A* **47** (2011) 148 [[1107.4388](#)].
- [62] M. Della Morte, A. Francis, V. Gülpers, G. Herdoíza, G. von Hippel, H. Horch et al., *The hadronic vacuum polarization contribution to the muon  $g - 2$  from lattice QCD*, *JHEP* **10** (2017) 020 [[1705.01775](#)].
- [63] BABAR collaboration, J. P. Lees et al., *Measurement of the spectral function for the  $\tau^- \rightarrow K^- K_S \nu_\tau$  decay*, *Phys. Rev. D* **98** (2018) 032010 [[1806.10280](#)].

- [64] BABAR collaboration, B. Aubert et al., *Measurements of  $e^+e^- \rightarrow K^+K^-\eta$ ,  $K^+K^-\pi^0$  and  $K_s^0K^\pm\pi^\mp$  cross-sections using initial state radiation events*, *Phys. Rev. D* **77** (2008) 092002 [[0710.4451](#)].
- [65] BABAR collaboration, J. P. Lees et al., *Cross Sections for the Reactions  $e^+e^- \rightarrow K^+K^-\pi^+\pi^-$ ,  $K^+K^-\pi^0\pi^0$ , and  $K^+K^-K^+K^-$  Measured Using Initial-State Radiation Events*, *Phys. Rev. D* **86** (2012) 012008 [[1103.3001](#)].
- [66] P. A. Baikov, K. G. Chetyrkin and J. H. Kuhn, *Order  $\alpha_s^4$  QCD Corrections to  $Z$  and  $\tau$  Decays*, *Phys. Rev. Lett.* **101** (2008) 012002 [[0801.1821](#)].
- [67] D. Boito, M. Golterman, K. Maltman, S. Peris, M. V. Rodrigues and W. Schaaf, *Strong coupling from an improved  $\tau$  vector isovector spectral function*, *Phys. Rev. D* **103** (2021) 034028 [[2012.10440](#)].
- [68] D. Boito, M. Golterman, A. Keshavarzi, K. Maltman, D. Nomura, S. Peris et al., *Strong coupling from  $e^+e^- \rightarrow$  hadrons below charm*, *Phys. Rev. D* **98** (2018) 074030 [[1805.08176](#)].
- [69] BES collaboration, J. Z. Bai et al., *Measurements of the cross-section for  $e^+e^- \rightarrow$  hadrons at center-of-mass energies from 2-GeV to 5-GeV*, *Phys. Rev. Lett.* **88** (2002) 101802 [[hep-ex/0102003](#)].
- [70] BES collaboration, M. Ablikim et al.,  *$R$  value measurements for  $e^+e^-$  annihilation at 2.60-GeV, 3.07-GeV and 3.65-GeV*, *Phys. Lett. B* **677** (2009) 239 [[0903.0900](#)].
- [71] KEDR collaboration, V. V. Anashin et al., *Precise measurement of  $R_{uds}$  and  $R$  between 1.84 and 3.72 GeV at the KEDR detector*, *Phys. Lett. B* **788** (2019) 42 [[1805.06235](#)].
- [72] BESIII collaboration, M. Ablikim et al., *Measurement of the Cross Section for  $e^+e^- \rightarrow$  hadrons at Energies from 2.2324 to 3.6710 GeV*, *Phys. Rev. Lett.* **128** (2022) 062004 [[2112.11728](#)].
- [73] M. Hoferichter, G. Colangelo, B.-L. Hoid, B. Kubis, J. R. de Elvira, D. Schuh et al., *Phenomenological Estimate of Isospin Breaking in Hadronic Vacuum Polarization*, *Phys. Rev. Lett.* **131** (2023) 161905 [[2307.02532](#)].
- [74] G. Colangelo, M. Hoferichter, B. Kubis and P. Stoffer, *Isospin-breaking effects in the two-pion contribution to hadronic vacuum polarization*, *JHEP* **10** (2022) 032 [[2208.08993](#)].
- [75] M. Hoferichter, B.-L. Hoid, B. Kubis and D. Schuh, *Isospin-breaking effects in the three-pion contribution to hadronic vacuum polarization*, *JHEP* **08** (2023) 208 [[2307.02546](#)].
- [76] FERMILAB LATTICE, LATTICE-HPQCD, MILC collaboration, C. T. H. Davies et al., *Hadronic-vacuum-polarization contribution to the muon's anomalous magnetic moment from four-flavor lattice QCD*, *Phys. Rev. D* **101** (2020) 034512 [[1902.04223](#)].



- [77] D. Giusti, F. Sanfilippo and S. Simula, *Light-quark contribution to the leading hadronic vacuum polarization term of the muon  $g - 2$  from twisted-mass fermions*, *Phys. Rev. D* **98** (2018) 114504 [[1808.00887](#)].
- [78] D. Giusti, V. Lubicz, G. Martinelli, F. Sanfilippo, S. Simula and C. Tarantino, *HVP contribution of the light quarks to the muon  $(g - 2)$  including isospin-breaking corrections with Twisted-Mass fermions*, *PoS LATTICE2018* (2018) 140 [[1810.05880](#)].
- [79] PACS collaboration, E. Shintani and Y. Kuramashi, *Hadronic vacuum polarization contribution to the muon  $g - 2$  with 2+1 flavor lattice QCD on a larger than  $(10 \text{ fm})^4$  lattice at the physical point*, *Phys. Rev. D* **100** (2019) 034517 [[1902.00885](#)].
- [80] S. Kuberski, on behalf of the Mainz collaboration, private communication (2024) .
- [81] C. T. H. Davies, A. S. Kronfeld, G. P. Lepage, C. McNeile and R. S. Van de Water, *Utility of a hybrid approach to the hadronic vacuum polarisation contribution to the muon anomalous magnetic moment*, [2410.23832](#).
- [82] D. Boito, M. Golterman, K. Maltman and S. Peris, *Spectral-weight sum rules for the hadronic vacuum polarization*, *Phys. Rev. D* **107** (2023) 034512 [[2210.13677](#)].